Structurally Confined Transition-Metal Oxide Layers, Chains and Oligomers in Molecular and Extended Magnetic Solids

Shiou-Jyh Hwu

Department of Chemistry and Materials Science & Engineering Program, Clemson University, Clemson, South Carolina 29634-1905

Received April 1, 1998. Revised Manuscript Received July 1, 1998

In an attempt to abstract the structural units of widely known silicate, phosphate, and arsenate compounds based on a transition-metal oxide (TM oxide) framework, we have gained some new insight into the study of "nanostructured" materials and their corresponding electronic and magnetic properties. In this review, we highlight some of the features associated with the nanosized TM oxide frameworks observed in this special class of oxides. Structurally, these oxides adopt a mixed framework that is composed of interlinked MO_6 (M = transition-metal cation) octahedra and XO_4 (X = Si^{4+}, P^{5+}, As^{5+}) tetrahedra. TM oxide octahedra may share vertexes, edges, and faces to form nanoscale layers, chains, and oligomers. These structurally well-defined low-dimensional lattices are of experimental and theoretical importance in the sense that electron interaction can be studied in a confined space. In this review, we will illustrate these structurally confined TM oxide frameworks, including those observed in molecular complexes.

Contents

Introduction

Transition-metal (TM) oxides have long provided both chemists and physicists with attractive solids that merit experimental and theoretical studies of technologically important phenomena. This already rich oxide system has once again received an enormous amount of attention since the discoveries of high-T_c superconducting cuprates by Bednorz and Müller[1] and by Chu and Wu.[2] The variety and complexity of the newly discovered oxides[3] and the evaluation of the factors that influence and control structural and physical properties have promoted renewed excitement in the study of TM oxides. Understanding fundamental parameters that govern the materials' performance has played a crucial role in every aspect of this research. Attempts to physically and/or chemically build nanometer-size structures are being made with the aim of simplifying the extended structures to reveal parameters that may be used to fine-tune the bulk physical properties.

Recent advances in the production of "nanostructured materials" by researchers studying condensed matter as well as molecular science have provided substances with some spectacular magnetic and electronic properties arising from quantum effects.[4−7] The solid-state physicist relies on methods for "physically" dividing bulk magnetic materials into their component nanometer-sized particles while trying to maintain control over their size, shape, and crystal structures. The synthetic chemist approaches the problem by attempting to build up well-defined small molecules having large numbers of unpaired spins. By incorporating spin-containing moieties into appropriate extended structures, cooperative magnetic coupling can be achieved to yield solid-state materials with reproducible properties.

This review will look at some transition-metal oxides containing silicates, phosphates, and arsenates, long-studied families of oxides that can provide both the chemist and physicist with the opportunity to study delocalized electrons in a confined lattice. In studying this class of solids, we have come to realize that the lattice confinement may be accomplished chemically by chelation with closed-shell, nonmagnetic oxyanions (XO_x^{n-}, X = Si, P, As). In the following discussions, we will also briefly contrast some of the chemically dissimilar higher nuclearity molecular complexes recently reported. The molecular solids, in principle, demonstrate the same feasibility of using organic-based, closed-shell ligands to achieve structural isolation and electronic insulation of TM-oxide-based magnetic clusters. This class of compounds, however, provides a less rigid lattice, which will give rise to less comparable spin−lattice interaction than the extended inorganic solids.

To further illustrate the concept, Figure 1 presents schematic drawings of idealized features containing confined TM oxide wires (chains) and sheets (layers) that are embedded in oxyanion-based insulating materials. These "composite" features are different than those seen in the nanostructured magnetic composite materi-

10.1021/cm980232l CCC: $15.00
Published on Web 09/25/1998

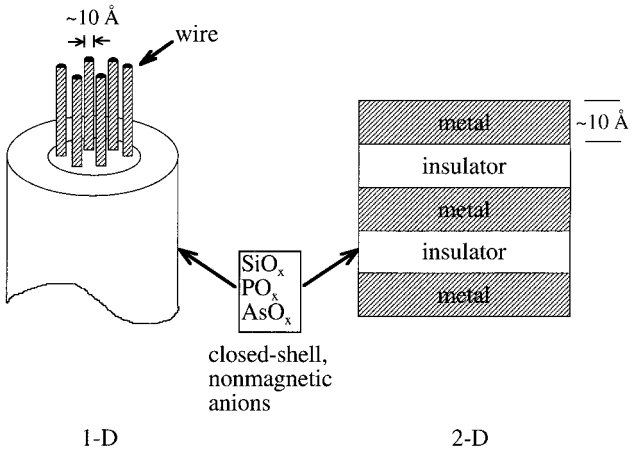

Figure 1. Nanosized transition-meta oxide wires (chains, left) and sheets (layers, right) are embedded in closed-shell, oxyanion-based matrix; see the text.

als because the bonding at the interface where two sublattices are combined is largely covalent. The TM oxide frameworks in question are, for the sake of description, approximately 10 Å (one nanometer) in size along the confined dimension(s). These confined TM oxide frameworks will be referred to hereafter as nanosized TM oxide layers, chains, or oligomers, depending on size and geometry.

The TM oxide lattice is generally constructed through the condensation of metal (M)-centered MO_6 octahedra, MO_4 tetrahedra, or related MO_5 square pyramids and trigonal bipyramids as well as MO_4 square planes. The resulting lattice contains M−O−M linkages and possibly M−M interactions. The following schematic drawings show the octahedral condensation in three different ways, in which the M center for each idealized octahedron is omitted for clarity. The vertex-sharing octahedra (**I**), as one can imagine, will result in a linear M−O−M linkage. The edge-sharing (**II**) and face-sharing (**III**) octahedra will each give a relatively short M−M distance in addition to a M−O−M linkage with a bent angle. The d_{M-M} calculated from idealized octahedra is expected to be 2.83 or 2.31 Å, respectively, based upon d_{M-O} being ca. 2.0 Å. It is rare to see face-sharing octahedra due to a short M−M distance and subsequently a strong cation−cation repulsion.

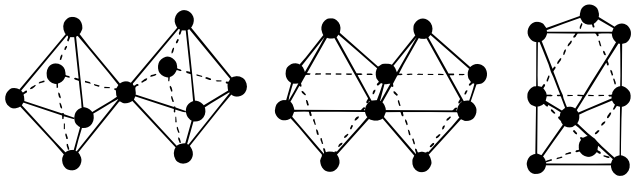

In the following sections, I will only discuss, due to space limitations, the synthesis of the aforementioned solid-state oxides made by the halide-flux methods. I will describe two useful methods for property characterization of this class of solids. A list of compounds based on nanosized TM oxides of Ti (d^1), Mn (d^{3-5}) or Cu (d^9) is given in an attempt to show their variety. Again, due to limited space, only a few examples from the list are selected for discussion of structure and, if possible, properties. In the conclusion, I will comment on some future directions to give some new insights into the study of "nanostructured" transition-metal oxide materials.

Synthesis via Halide Flux Methods

The growth of single crystals is important in order to avoid problems associated with grain boundaries and random orientation of crystal lattices in polycrystalline materials. Single crystals are necessary in this research because they have been used to determine not only the crystal structure, but also the anisotropic magnetic and transport properties.

The fruitful structural chemistry demonstrated in our exploratory synthesis is due largely to the employment of molten halide fluxes. It is evident that these halides are a good reaction medium for the crystal growth of refractory compounds. A wide spectrum of halide fluxes, alkali and alkaline-earth halides, provides a sizable temperature window (300−1000 °C) for synthesis and crystal growth.[8] These fluxes include single salts, such as the monochlorides A^ICl (mp = 605 °C for LiCl up to 801 °C for NaCl) and dichlorides $A^{II}Cl_2$ (mp = 782 °C for $CaCl_2$ up to 963 °C for $BaCl_2$), and eutectic mixtures such as $CaCl_2/BaCl_2$ (mp = 450 °C for 43.6/56.4 molar ratio). While the role of molten halides needs to be studied further, these flux techniques (in contrast to traditional, high-temperature, solid-state synthesis) allow new discoveries to be made through altered reaction conditions, such as acidity and basicity, solubility, and reaction temperature. It is realized that incidental incorporation of cations and/or anions from the flux is inevitable. The salt inclusion, however, provides much variety in the structural features of the final product.[9] In any case, these fluxes are inexpensive and have proven to be easy to work with in terms of retrieving crystals.

The flux-growth reaction can be performed in a carbon-coated fused silica ampule. The halide salt is added to the reactants in a mass ratio of 3−10:1 as a flux for crystal growth. The reaction mixture is sealed inside a quartz container which is carbon coated by the pyrolysis of acetone or ethanol. It is then heated at the desired temperature, typically 100−200 °C above the melting point of the flux, for ca. 1−2 weeks, followed by slow cooling at a rate of 2−25 °C/h to ∼50 °C below the melting point of the flux, and then the furnace is cooled to room temperature. Single crystals are retrieved by washing the product with deionized water using suction filtration.

Property Characterization

Several techniques suitable for measuring bulk physical properties of conventional solid-state compounds may not be applicable for the property characterization of some of these compounds. Measuring electrical conductivity, for example, is impractical for solids containing a "discrete" TM oxide framework. Magnetic susceptometry, however, would be an invaluable tool for the study of magnetochemistry and electronic properties of molecular solids and solids containing confined TM oxide lattices, like the ones mentioned in this review. UV−vis spectroscopy would be useful for the routine analysis of the electronic structure of this class of solids (see the later example).

Table 1. Selected Examples of Manganese-Based Higher Nuclearity Complexes[a]

complex	$[M_xO_y]^{n+}$ core	ground state S	ref
$[Mn_{12}O_{12}(O_2CPh)_{16}(H_2O)_4]$	$[Mn_{12}O_{12}]^{16+}$	14	25
$[Mn_{10}O_8(O_2CPh)_6(pic)_8]\cdot 3H_2O$	$[Mn_{10}O_8]^{14+}$	NA	26
$(NEt_4)[Mn_7O_4(OAc)_{10}(dbm)_4]$	$[Mn_7O_4]^{13+}$	3−4	27
$(NBu^n_4)_2[Mn_8O_4(O_2CPh)_{12}(Et_2mal)_2(H_2O)_2]\cdot CH_2Cl_2$	$[Mn_8O_4]^{14+}$	3	28
$[Mn_9O_7(O_2CC_6H_5)_{13}(py)_2]$	$[Mn_9O_7]^{13+}$	NA	30
$[Mn_9O_7(O_2CPh)_8(sal)_4(salH)_2(pyr)_4]$	$[Mn_9O_7]^{12+}$	NA	29
$[Mn_{10}O_{14}\{N(CH_2CH_2NH_2)_3\}_6]^{8+}$	$[Mn_{10}O_{14}]^{8+}$	NA	31
$[Mn_{10}(biphen)_4O_4Cl_{12}]^{4-}$	$[Mn_{10}O_4]^{16+}$	13−14	35
$(Et_4N)_2[Mn_{10}O_2Cl_8\{(OCH_2)_3CMe\}_6]\cdot 4MeOH\cdot 2H_2O$	$[Mn_{10}O_{20}]^{12-}$	NA	36
$K_4[Mn_{18}O_{16}(O_2CPh)_{22}(phth)_2(H_2O)_4]\cdot 10MeCN$	$[Mn_{18}O_{16}]^{22+}$	11	37
$(PPh_4)[Mn_{12}O_{12}(O_2CEt)_{16}(H_2O)_4]$	$[Mn_{12}O_{12}]^{15+}$	9−10	38
$[Mn_2L)_6(OH)_4(CH_3CO_2)_2]$, L = $C_{21}H_{15}N_2O_3$	$[Mn_{12}L_6]^{4+}$	NA	39
$[Mn_{13}O_8(OEt)_6(O_2CPh)_{12}]$	$[Mn_{13}O_8(OEt)_6]^{12+}$	$^{15}/_2$	40
$[(NBu^n_4)[Mn_8O_6Cl_6(O_2CPh)_7(H_2O)_2]$	$[Mn_8O_6]^{12+}$	11	41
$[Mn_9Na_2O_7(O_2CPh)_{15}(MeCN)_2]$	$[Mn_9O_7]^{13+}$	4	41
$[Mn_{12}O_{12}(O_2CR)_{16}(H_2O)_4]$ [R = Ph, Me, Et]	$[Mn_{12}O_{12}]^{16+}$	$^{19}/_2$ (R = Et)	42, 43
$[Mn_{12}(CH_3COO)_{16}(H_2O)_4O_{12}]$	$[Mn_{12}O_{12}]^{16+}$	NA	44
$[Mn_{10}O_4(biphen)_4X_{12}]^{4-}$ (X = Cl^-, Br^-)	$[Mn_{10}O_4]^{16+}$	$12 \le S \le 14$	45
$[Mn_{16}Ba_8Na_2ClO_4(OH)_4(CO_3)_4(H_2O)_{22}L_8]$		NA	46

[a] For the purpose of this discussion, "high-nuclearity complexes" are defined as those with seven or more metal atoms. The smaller complexes can be found in ref 23 and references therein.

A recent study of temperature-dependent magnetic properties of three transition-metal arsenates of this type by Nakua and Greedan has shown some intriguing results. In their report, they find no evidence of the presence of any short-range magnetic order between isolated magnetic centers.[10] These compounds are divalent transition-metal arsenates with the general formula MAs_2O_6, where M is Mn, Co, or Ni. The framework adopts a hexagonal close-packed network of oxygen atoms, and alternate layers of octahedral sites are filled two-thirds by As^{5+} ions and one-third by the M^{2+} ions. This leads to sheets of edge-sharing AsO_6 octahedra, while the transition-metal ions are located in isolated octahedral sites. The Curie−Weiss fits present no deviations at lower temperatures. The absence of any significant short-range order correlations in these oxides is discussed due to the absence of a dominating superexchange M−O−M pathway. All three compounds, otherwise, exhibit what appears to be a magnetic long-range order transition at low-temperatures. In $BaTi_2(P_2O_7)_2$, for example, we have observed similar magnetic properties which indicate that electron localization in isolated magnetic centers is indeed possible due to the closed-shell, nonmagnetic oxyanions.[11,12]

UV−vis spectroscopy is a convenient tool to identify the discrete nature of the nanosized TM oxide framework. There are three major transitions one would expect. The absorption due to the d−d transitions can be detected at roughly ∼1−2 eV (∼1240−620 nm).[13a] The absorption corresponding to LMCT bands originating from the XO_4 group can be observed at ca. 3 eV (∼413 nm) and above. The absorption resulting from the bridging oxo oxygen (M−O−M) LMCT band can be seen at the low-energy region between the first two transitions.[13b,c]

On Molecular Complexes with $[M_xO_y]^{n+}$ Core

Molecular complexes have the advantage of a single, crystallographically defined size, unlike many nanoscale magnetic materials which have a distribution of cluster sizes.[6,7,14−23] The discrete nature of this structural property gives, in principle, many possibilities to modulate the bulk physical properties of the material by appropriately choosing the constituent molecules.[14] The bulk properties are often determined by cooperative interactions between the constituent molecules, which consequently can be assembled in the lattice in such a way to maximize the bulk response. Some molecular magnets showing interesting ferro- and antiferromagnetic interactions have been observed in some recent examples of Ni- and Cu-based molecular complexes.[15−19]

We will briefly describe the Mn-based molecular complexes in this section for the future comparison of nanosized Mn−O framework between molecular and extended solids. The primary interest of these studies has been stimulated by a number of factors, including the aesthetically pleasing structures of the $[M_xO_y]^{n+}$ core and their propensity to exhibit attractive magnetic properties due to a high-spin ground state S. Efforts have been initially directed primarily toward di- and tetranuclear species to obtain potential models of the Mn units within certain manganese biomolecules.[23] The structure of $Mn_4O_3Cl_4(O_2CR)_3(py)_3$, for example, possesses a $[Mn_4O_3]^{7+}$ "partial cubane" unit with the vacant apex occupied by a μ_3-Cl^- ion.[24] The compounds reported in ref 23 are high-spin and the exchange interactions are relatively small. In most cases, they are antiferromagnetic (negative J). Some rare examples are ferromagnetic (positive J), which has led to high spin ground states. One of the most noteworthy species is the $Mn_{12}O_{12}(O_2CPh)_{16}(H_2O)_4$ complex, whose remarkable spin ground state of $S = 14$ is the highest yet observed for a discrete molecule.[25] The complex consists of a central $Mn^{IV}_4O_4$ cubane held within a nonplanar ring of eight Mn^{III} atoms by eight μ_3-oxide atoms.

Manganese carboxylate chemistry continues to be a source of cluster complexes with a variety of metal nuclearities up to 18 (Table 1).[26−31,35−46] The oxidation states of magnetic manganese in these complexes range from II to IV. Figure 2 shows the partial structure of a discrete polyoxomanganese cation $[Mn_{10}O_{14}(tren)_6]^{8+}$,[31] whose $Mn_6O_{14}N_8$ core resembles in some respect the layered structures of extended solids of the naturally occurring manganese oxide minerals chalcophanite ($ZnMn_3O_7\bullet 3H_2O$)[32,33] and lithiophorite ($(Al,Li)MnO_2$-

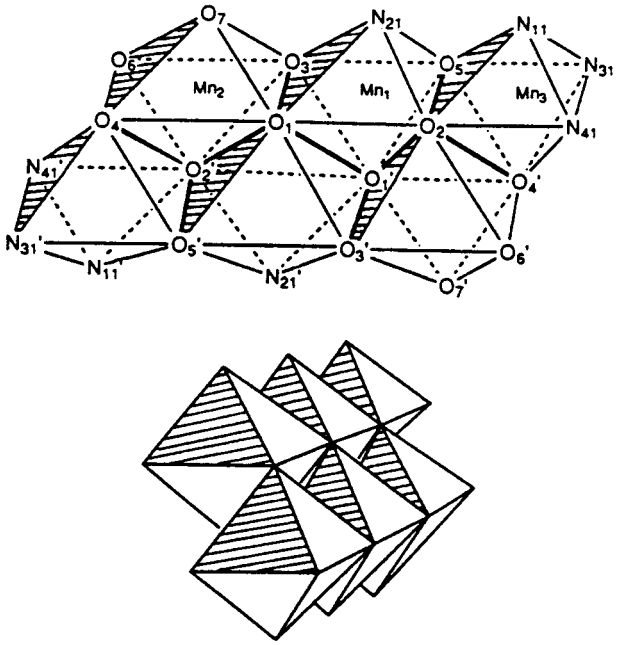

Figure 2. Top view showing $Mn_6O_{14}N_8$ core made of edge-sharing octahedra in the $[Mn_{10}O_{14}(tren)_6]^{8+}$ structure. At the bottom is an oblique view showing the layered nature of edge-sharing octahedra. (Reprinted with permission from ref 31.)

$(OH)_2$).[33,34] Relatively few examples show magnetic susceptibilities increasing with decreasing temperature, e.g. $(Me_4N)_4[Mn_{10}(biphen)_4O_4Cl_{12}]$,[35] $(NBu^n_4)[Mn_8O_6Cl_6(O_2CPh)_7(H_2O)_2]$,[41] and $Mn_{12}O_{12}(O_2CR)_{16}(H_2O)_4$ (R = Ph, Me, Et).[42,43] The later three mixed-valent $Mn^{IV}_4Mn^{III}_8$ complexes show a maximum ($19-20\mu_B$) in μ_{eff}/molecule vs. temperature at 10−20 K. This is attributed to the population of a large-spin ground state at the lowest temperatures.

Figure 3 shows the $[Mn_{10}O_{20}Cl_8]$ core of the $[Mn_{10}O_2Cl_8\{(OCH_2)_3CMe\}_6]^{2-}$ complex anion. The structure of the core contains edge-shared MnL_6 (L = O, Cl) octahedra which adopt a characteristic feature of condensed oxides.

A Mn_{13} complex containing a novel supercubane $[Mn^{IV}Mn^{III}_6Mn^{II}_6(\mu_5\text{-}O)_6(\mu_3\text{-}OEt)_6]^{12+}$ core has been isolated recently.[40] Figure 4 shows the structural framework of $[Mn_{13}O_{14}]$ that adopts a distorted structure mimicking the unit cell of NaCl.

Molecular complexes that have metal cations that adopt several oxidation states exhibit interesting properties. The crystal structure of $(PPh_4)[Mn_{12}O_{12}(O_2CEt)_{16}(H_2O)_4]$ shows a localized-valence Mn^{II}, $7Mn^{III}$, $4Mn^{IV}$ situation. Dc and ac magnetic susceptibility studies show that this complex has an $S = {}^{19}/_2$ ground state and that it displays a superparamagnet-like nonzero frequency-dependent out-of-phase response in the ac susceptibility behavior that is unusual for a molecular species and unique for an ionic species.[38]

The general synthetic strategies of higher nuclearity complexes have been demonstrated beautifully by dissolution of preformed, small nuclearity species with $[Mn_3O]^{6+,7+}$ or $[Mn_4O_2]^{8+}$ cores followed by reprecipitation (aggregation).[23] For example, reaction of $[Mn_4O_2(O_2CMe)_6(py)_2(dbm)_2]$ (dbm^- is the anion of dibenzoylmethane) with Cl^- in CH_2Cl_2 gives the heptanuclear complex $[Mn_7O_4(O_2CMe)_{10}(dbm)_4]^-$,[27] and reaction of

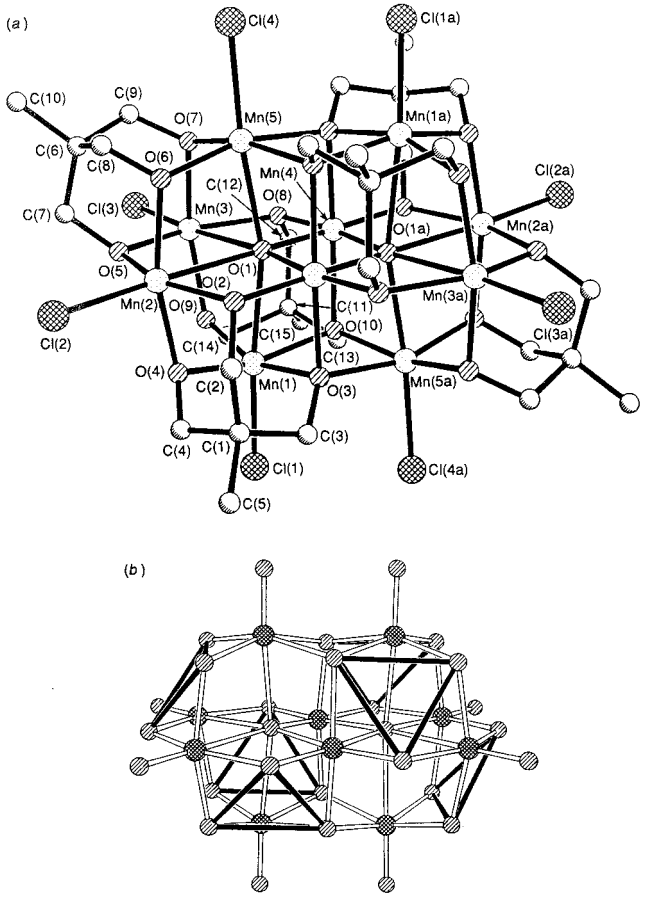

Figure 3. (a) A view of the $[Mn_{10}O_{20}Cl_8]$ core of the $[Mn_{10}O_2Cl_8\{(OCH_2)_3CMe\}_6]^{2-}$ structure. (b) Schematic representation of the $\{M_{10}L_{28}\}$ core. (Reprinted with permission from ref 36.)

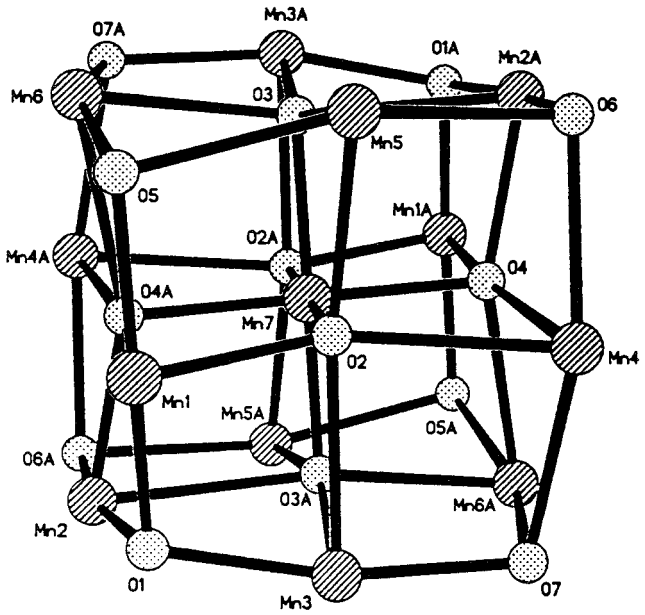

Figure 4. The NaCl-type $[Mn_{13}O_{14}]$ core in the novel supercubane $[Mn^{IV}Mn^{III}_6Mn^{II}_6(\mu_5\text{-}O)_6(\mu_3\text{-}OEt)_6]^{12+}$ complex. (Reprinted with permission from ref 40.)

$[Mn_4O_2(O_2CPh)_9(H_2O)]^-$ with Me_3SiCl gives the octanuclear complex $[Mn_8O_6Cl_6(O_2CPh)_7(H_2O)_2]^-$.[41] Similarly, treatment of $[Mn_4O_2(O_2CPh)_9(H_2O]^-$ with Khphth ($Hphth^-$ is monodeprotonated phthalic acid) gives K_4-

$Mn_{18}O_{16}(O_2CPh)_{22}(phth)_2(H_2O)_4$.[37] Aggregation via dissolution of $[Mn_4O_2(O_2CPh)_6(MeCN)_2(pic)_2]$ in $MeCONMe_2$ (DMA) and CH_2Cl_2 in the presence of picH (picolinic acid) leads to slow crystallization of $[Mn_{10}O_8(O_2CPh)_6(pic)_8]$.[26]

On Extended Solids

The chemistry of transition-metal-containing silicates, phosphates, and arsenates discussed in this section has an ancient history and has been studied mostly by mineralogists. The structures of these families of oxides are complex and have been abstracted almost exclusively from the point of view of the extended X−O (X = Si, P, As) lattice. The transition-metal cation in these lattices has been viewed as a linker to the building blocks of the extended oxide framework, and it has received little attention with regard to the role that it plays in governing physical properties of electronic and magnetic importance. In light of the potential features offered by oxyanions for lattice confinement, we will revisit some of these solids from a different structural point of view. In this review, their nanometer-sized, transition-metal oxide layers, chains, and clusters will be emphasized.

As expected, the database for the TM−X−O based minerals is large.[47] If we limit our search of existing materials to compounds that contain just six or fewer elements, we find a total of 682 phases, which include three families of compounds, 196 of which have TM = Ti, 282 with TM = Mn, and 204 with TM = Cu. The reason that these three elements are chosen here is mainly because they represent the chemistry of silicates, phosphates, and arsenates of early, middle, and late transition-metal cations that we have been studying. Some of our recent findings, with regard to the specific TM oxide frameworks, will also be included in the following discussions.

Titanium-Containing Compounds. Thus far, much of our effort has involved the synthesis of mixed-valence early transition-metal (d^{0-2}) phosphates and silicates. A novel family of quasi-two-dimensional oxosilicates has been discovered. The structural formula of this compound series can be written as $La_4M(Si_2O_7)_2(MO_2)_{4m}$,[12,48] where m (=1, 2) represents the thickness of the (110) MO_2 (M = Ti, V) rutile layer (see the structure of $La_4Ti_9Si_4O_{30}$ titanium(III/IV) phase (m = 2) in Figure 5). The extended framework consists of alternating slabs of $(TiO_2)_{4m}$ and $La_4Ti(Si_2O_7)_2$ silicate layers. Band structure calculations show that the d electrons reside entirely in the rutile layers, and the bottom portions of their d-block bands are partially filled.[48d] Conductivity measurements on pressed-pellet samples of the Ti series show semiconducting behavior with small gap energies and exhibit a sharp transition at low temperatures. This indicates that the electrons in the partially filled bands are localized. The electronic band structures and bonding analyses of the m = 1 and 2 phases suggest that bipolaron formation is likely causing the electron localization and, thus, the observed nonmetallic state.

It is likely that any transition-metal dioxide MO_2 adopting the rutile structure[49] should form $La_4M(Si_2O_7)_2(MO_2)_{4m}$. In fact, recent reports on $La_{3.4}Ca_{0.6}V_5Si_4O_{22}$[48b] and $La_4M_5Si_4O_{22}$ (M = V, Mn)[48e] demonstrate that rutile sheets of both early transition-metal (V) oxide and middle transition-metal (Mn) oxide can be incorporated. This facilitates systematic studies of electron interactions in a confined lattice at different d electron levels.

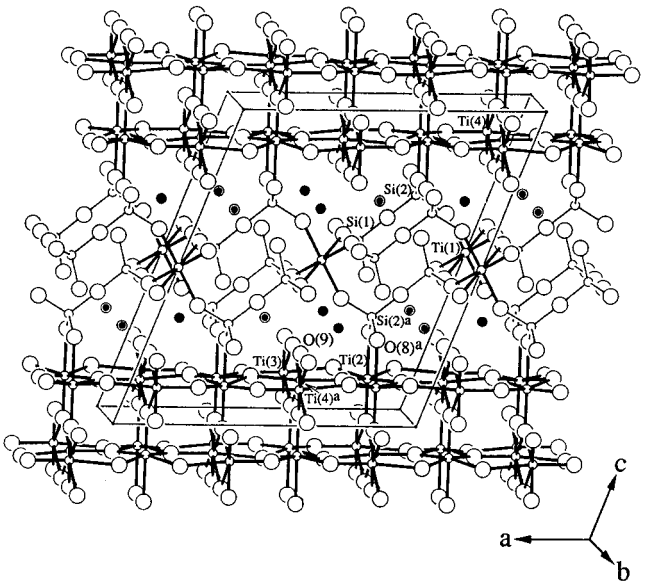

Figure 5. Structure of α-$La_4Ti_9Si_4O_{30}$ viewed approximately along the *b* axis of the monoclinic unit cell, as outlined. All the octahedral coordinations in TiO_6 are represented by thick lines and the tetrahedral coordinations in Si_2O_7 by thin lines. Small circles represent titanium and silicon atoms and large circles represent oxygen atoms, whereas small solid circles represent the lanthanum atoms. (Reprinted with permission from ref 48d.)

Fascinating structural chemistry has been observed in this oxosilicate series. Two new polymorphs, α- and β-$La_4Ti_9Si_4O_{30}$, show structures which can be considered diastereomeric, with respect to the relative orientations of rutile and silicate slabs. While the orientation of the rutile slab is fixed, the silicate slabs in these structures are mirror images of each other. The observed difference in the unit cell dimension c (15.189 Å vs 14.252 Å) and monoclinic angle β (110.92° vs 95.39°) is the result of lattice matching. Taking into account the difference in the tilted angle β, the spacing between the rutile slabs ($d_{001} \equiv c \times \sin \beta$) is essentially the same, 14.187 Å vs 14.189 Å, respectively. Also, the cation-substituted $La_4Ti_5Si_{4-x}P_xO_{22}$ series (m = 1) can be prepared. This mixed-silicophosphate family lends additional merit to our systematic study with regard to the ability to fine-tune the electronic structure of the rutile sheet without introducing structural variation.

Manganese(II,III,IV)-Containing Silicates, Phosphates, Arsenates. Many minerals not only have attractive X−O frameworks but also contain novel TM oxide lattices that are embedded in the X−O matrix. The formulas and structures are often complex due to cation mixing in a common crystallographic site (Table 2).[50−87] Inesite, for example, has a relatively simple chemical formula, $Ca_2Mn_7Si_{10}O_{28}(OH)_2 \cdot 5H_2O$, and, incidentally, an interesting three-dimensional framework.[59] The extended framework contains double silicate chains with a five-tetrahedron-repeat period, which consists of alternating six- and eight-membered rings. The embedded Mn−O lattice, which forms an edge-

Table 2. A Partial List of Silicate, Phosphate, and Arsenate Compounds Containing Mn−O Oligomers, Chains, and Sheets

compound	special frameworks	property	ref
	Oligomers		
$AMnP_2O_7$ (A = Ca, Ba)	edge-sharing Mn_2O_{10}	antiferromagnetic	52
$Na_2MnP_2O_7$	edge-sharing Mn_2O_{10}	antiferromagnetic	53
$CaMn_2(BeSiO_4)_3$	face-sharing Mn_2O_9, d_{Mn-Mn} = 3.25 Å		56
Mn_7SbAsO_{12}, manganostibite	edge-sharing Mn_2O_{10} and Mn_3O_{14} octahedral units		65
$LiNaMn_8Si_{10}O_{28}(OH)_2$, nambulite	cross-linked, six edge-sharing MnO_6 octahedral units		66
$Ca_2Mn_7Si_{10}O_{28}(OH)_2 \cdot 5H_2O$, inesite	cross-linked, seven edge-sharing MnO_6 octahedral units		59
$Ca_2Mn_8Si_{10}O_{30}$, rhodonite	cross-linked, eight edge-sharing MnO_6 octahedral units		60
$CaMn(HAsO_4)_2(H_2O)_2$	edge-shared MnO_6 dimer		70
$K_2Mn_2Zn_4Si_4O_{15}$	edge-shared MnO_5 dimer		77
$LiMnPO_4$	edge-shared MnO_6 dimer		87
	Chains		
$Cu_2Mn(PO_4)_2(H_2O)$	parallel double chains of $CuO_4/CuO_4(H_2O)/MnO_5(H_2O)$		51
$BaSr_2Mn_2O_2(Si_4O_{12})$	MnO_6 octahedral chain		54
$NaMn_3(PO_4)(HPO_4)_2$	MnO_6 octahedral chain	antiferromagnetic, d^5 high spin	57
$Ca_3Mn_2O_2(Si_4O_{12})$	MnO_6 octahedral chain		54
$KMn_2O(PO_4)(HPO_4)$	edge-sharing MnO_6 zigzag chain		58
$NH_4Mn_2O(PO_4)(HPO_4) \cdot H_2O$	edge-sharing MnO_6 zigzag chain		64
$NaMnSi_2O_6$	edge-sharing MnO_6 zigzag chain		67
$Na_{2.29}Mn_{10}(Si_{11}VO_{34})(OH)_4$	edge-shared MnO_6		69
$Na_2Mn_2Si_2O_7$	vertex- and edge-shared MnO_6		73
$CaMn_4Si_5O_{15}$	edge-shared MnO_6		75
$Na_2MnIn(SiO_3(OH))_2(OH)$	edge-shared MnO_6		78
$SrMn_2(Si_2O_7)(OH)_2(H_2O)$, lawsonite	edge-shared MnO_6		83
$CaMnSi_2O_6$	edge-shared MnO_6 zigzag chain		85
$NaMnPO_4$	edge-shared MnO_6 chain		86
	Sheets		
$KMnPO_4 \cdot H_2O$	vertex-shared MnO_6	magnetic data	50
$CuMn_2(PO_4)_2(H_2O)$	edge-shared $MnO_6/MnO_4(H_2O)_2$		51
$KLiMn_2Si_4O_{12}$	MnO_6 octahedra sharing *cis* edge		55
$Ca(Mn,Fe)_{14}SiO_{24}$, braunite II	edge- and vertex-shared $(Mn,Fe)O_6$ octahedra		61
$Mn_3(OH)_4(AsO_4)$, flinkite	edge-shared MnO_6 octahedra		63
$Pb_2Mn_2Si_2O_9$	vertex-shared MnO_6 octahedra		68
Mn_4SiO_7	face- and edge-shared MnO_6 octahedra		71
$K_2Mn_5(Si_{12}O_{30})(H_2O)$, milarite	edge-shared rings of alternating $6MnO_4$ and $6MnO_6$ sharing edges		76
$MnPO_4$	vertex-shared MnO_6		79
$LiMn(AsO_4)$	vertex-sharing MnO_6		80
	Mixed Frameworks		
$(Mn_2O_3)_3MnSiO_3$	MnO_8 and MnO_6 polyhedra		72
$MnSiO_3$	edge-sharing MnO_6		74
$KMn_4(PO_4)_3$	edge-shared MnO_6		81
$Cu_{2.5}Mn(PO_4)_2(OH)$	mixed framework of vertex- and edge-shared MnO_6 and CuO_n (n = 4−6)		82
$BaMn_2TiO(Si_2O_7)(OH)_2$	mixed framework of edge-shared MnO_6 sharing common vertexes with TiO_6		84

sharing polyhedral band, consists of a sequence of seven Mn(II) octahedra capped by two Ca pentagonal bipyramids to form the $Mn_7Ca_2O_{36}$ unit. The extended lattice propagates by cross-linking these units through sharing the cis edges of the four MnO_6 octahedra. The formation of a Mn-deficient, high-Ca rhodonite, $Ca_2Mn_7Si_{10}O_{29}$, has been demonstrated by dehydration of inesite followed by thermal migration (diffusion) of Ca^{2+} and Mn^{2+} cations via the octahedral band (see ref 59 and references therein). The regular rhodonite structure contains ten-octahedra $CaO_6/8MnO_6/CaO_6$ units and single silicate chains with a five-tetrahedron repeat.

Several investigated minerals contain novel transition-metal oxide frameworks. Mn milarite,[76] $K_2Mn_5(Si_{12}O_{30})(H_2O)$, for example, has extended sheets made of rings of alternating $6MnO_4$ and $6MnO_6$ polyhedra sharing edges (Figure 6). The Mn−O distances are 2.22 Å (×6) and 2.08 Å (×4), respectively. The Mn−Mn distance across the shared edge is 3.019 Å.

The A-site cation has a substantial effect on this type of mixed-framework compounds. The structures of the edge-shared zigzag chain of MnO_6 octahedra in the framework of taikanite,[54a] $BaSr_2Mn_2O_2(Si_4O_{12})$, and CMS-XI,[54b] $Ca_3Mn_2O_2(Si_4O_{12})$, are different due to the different A-site cations, $BaSr_2$ and Ca_3, respectively. CMS-XI is composed of undulating cis−trans−cis octahedral edge-sharing chains with a 10 Å translation period. In taikanite the sinusoidal undulating chains have a cis−cis connectivity with a 5.1 Å translation period.

Three new isotypic phosphates of the $A^I{}_2B^{II}P_2O_7$ type that adopt two dramatically different layered structures were reported recently.[53] $Na_2MnP_2O_7$ possesses a novel Mn−P−O slab structure made of fused $Mn_4P_4O_{26}$ cages (Figure 7). Due to the A-site cation effect, $NaCsMnP_2O_7$ and $NaCsMn_{0.35}Cs_{0.65}P_2O_7$ form the $K_2CuP_2O_7$ structure containing undulating slabs of corner-sharing MnO_5 and P_2O_7 units. The dimer-like, short-range ordering for the Mn_2O_{10} dimers is absent in the magnetic susceptibility of $Na_2MnP_2O_7$ (Figure 8a), instead the sharp maximum indicating antiferromagnetic transition at ∼7.2 K. The transition is completely missing in $NaCsMnP_2O_7$ (Figure 8b), likely because of the absence of a superexchange pathway Mn−O−Mn.

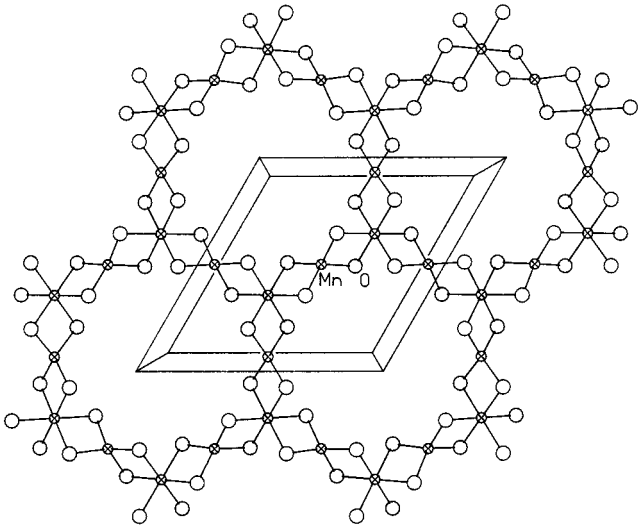

Figure 6. Ring of alternating $6MnO_4$ and $6MnO_6$ sharing edges of $K_2Mn_5(Si_{12}O_{30})(H_2O)$. The extended sheet is formed by sharing the edges of $2MnO_6$ and $1MnO_4$ of the neighboring rings.

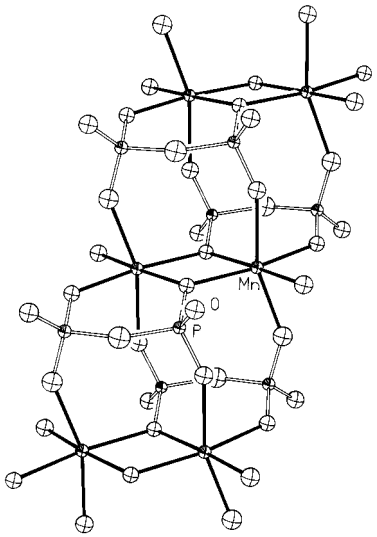

Figure 7. Two empty $Mn_4P_4O_{26}$ cages in $Na_2MnP_2O_7$ are fused by sharing a common Mn_2O_{10} dimer. Each cage is centered by the inversion center. The Mn_2O_{10} dimer is highlighted by solid lines and the P_2O_7 unit is outlined by hollow lines.

Copper-Based Silicates, Phosphates, Arsenates. Likewise, many minerals exhibit novel structures that contain interesting nanosized Cu−O frameworks. Table 3 lists some examples from a large class of existing compounds as well as some phases newly synthesized in our laboratory.[88−147] Figure 9 shows the structure of shattuckite, $Cu_5(SiO_3)_4(OH)_2$, which contains brucite-like $(CuO_2)_n$ layers built up from edge-shared octahedra.[102] The CuO_6 octahedron adopts the [4 + 2] Jahn−Teller distortion where the two long bonds are 2.59 Å ($k \times 2$, for Cu(1)), 2.62 Å, and 2.31 Å (P, Q for Cu(2)), much longer than 1.96 Å, 1.98 Å ($i \times 2$, $j \times 2$), and 1.93−2.05 Å (L∼O) of the four short bonds, respectively. The isolated square planar CuO_4 consists four regular Cu−O bonds, 1.89−1.95 Å (R∼U). In addition, the two long Cu−O are 2.69 and 2.78 Å (V, X for Cu(3)). The rows of planar CuO_4 groups in the layers are sharply tilted and interestingly arranged like Venetian blinds (Figure 10). The analogous planchéite possesses similar $(CuO_2)_n$ layers that are separated by different silicate groups.

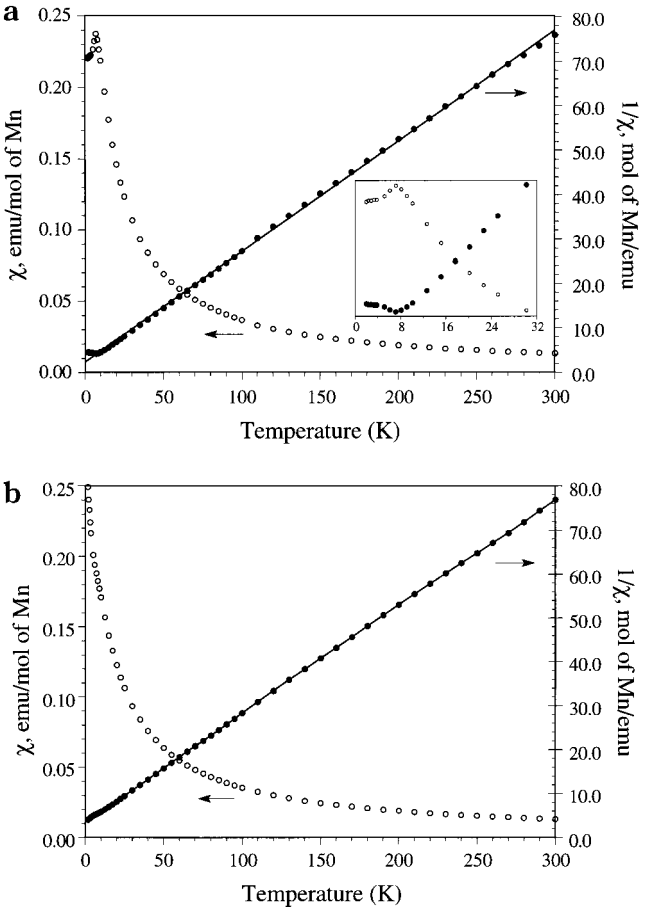

Figure 8. Magnetic susceptibility of (a) $Na_2MnP_2O_7$ and (b) $NaCsMnP_2O_7$.

Also, two novel phases, $Pb_2Cu^{II}_7(AsO_4)_6$ (**II**) and $Pb_2Cu^{I}_2Cu^{II}_6(AsO_4)_6$ (**I-II**), with topologically related crystal structures were recently discovered by Effenberger.[96] **II** contains $Cu^{II}_3O_{10}$ and $Cu^{II}_4O_{12}$ chains formed by edge and vertex connections of $Cu^{II}O_4$ squares and distorted $Cu^{II}O_5$ trigonal bipyramids. While the Cu_3O_{10} chain is maintained in **I-II**, the Cu_4O_{12} chain is interrupted by the substitution of the $Cu(1)O_4$ square by the two linearly coordinated monovalent copper atoms. The $O-Cu^{I}-O$ linkage connects the Cu_3O_{12} groups and the Cu_4O_{12} chains to form corrugated layers.

The magnetic properties of these Cu^{2+}-based silicates, including phosphates and arsenates in the same matter, are rarely studied. Studies of dioptase, $Cu_6[Si_6O_{18}]\cdot 6H_2O$, show that the three-dimensional lattice consists of corner-sharing Cu_2O_6 dimers that are made of pairs of edge-shared planar CuO_4 groups.[104] Magnetic studies reveal that the material becomes antiferromagnetic near 70 K.[105] The proposed magnetic structure based on a doubled unit cell ($c' = 2c = 15.60$ Å) suggests a superexchange via an extended antiferromagnetic ordering through Cu−O−Cu bridges.

It is relatively rare to find structures containing Cu−O chains. In the mixed sulfate and silicate mineral wherryite, $Pb_7Cu_2(SO_4)_4(SiO_4)_2(OH)_2$, the copper oxide framework forms a pseudo-one-dimensional chain.[107] Figure 11 shows the Cu−O chain made of [4 + 2] distorted octahedra. It is noted that the chains are

Table 3. A Partial List of Silicate, Phosphate, and Arsenate Compounds Containing Cu−O Oligomers, Chains, and Sheets

compound	special frameworks	property	ref
	Oligomers		
$Na_2Cu_3(Si_4O_{12})$	edge-shared Cu_2O_6 square planar dimer		88
$Li_2Cu_5(Si_2O_7)_2$	edge-shared Cu_2O_8 and Cu_3O_{10}		89
$Rb_2Cu_2Si_8O_{19}$	dimeric edge-shared Cu_2O_6 square planar polyhedra		93
$Cs_2Cu_2Si_8O_{19}$	dimeric edge-shared Cu_2O_6 square planar polyhedra		90
$Ba_2Cu_2(Si_4O_{12})$	edge-shared Cu_2O_6 dimer		92
$K_2Cu_3(As_2O_6)_2$	edge-shared Cu_3O_8 trimer		97
$BaCu_2(AsO_4)_2$	edge-shared Cu_2O_8 trigonal bipyramidal dimer		100
$CuAgH_3(AsO_4)_2$	edge-shared Cu_2O_8 square planar dimer		109
$Cu_2Al(AsO_4)(OH)_4 \cdot 4H_2O$	edge-shared Cu_2O_{10} octahedral dimer		111
$Li_2Cu_3(SiO_3)_4$	edge-shared Cu_3O_8 square planar trimer		this work
$ANa_5Cu_4(AsO_4)_4Cl_2$, A = Rb, Cs	vertex-shared Cu_4O_{12} cyclic tetramer		this work
$KCuPO_4$	vertex-shared CuO_4 and CuO_5		122
$Na_5Cu_3(PO_4)_2[(PO_4)HPO_4]$	Cu_3O_{12} unit of vertex-shared CuO_4 and $2CuO_5$		124
$Cu_3P_6O_{18} \cdot 14H_2O$	edge-shared Cu_2O_{10} octahedral dimer		127
$Ag_5Cu_3(PO_4)_2[(PO_4)HPO_4]$	Cu_3O_{12} unit of vertex-shared CuO_4 and $2CuO_5$		128
$Cu(HPO_3H)_2$	edge-shared Cu_2O_{10} octahedral dimer		129
$CuPO_3F \cdot 2H_2O$	edge-shared Cu_2O_8 square pyramidal dimer		130
$BaCuP_2O_7$	dimers of edge-shared square pyramidal CuO_5[4+1]		132
$Ca_3Cu_3(XO_4)_4$ (X = P, As)	vertex-shared $2CuO_5$[4+1] + CuO_4 trimer		140
$Li_2Cu_2P_6O_{18}$	edge-sharing CuO_6[4+2] dimer		141
$K_4Cu_3(AsO_4)_2[AsO_3(OH)]_2$	vertex-sharing $2CuO_5$[4+1] + CuO_4 trimer		144
	Chains		
$BaCu_2(PO_4)_2$	CuO_5 bipyramidal chain	anti, T_{max} = 65 K	103
$Pb_7Cu_2(SO_4)_4(SiO_4)_2(OH)_2$, wherryite	edge-shared CuO_6 [4+2] octahedral chain		107
$Li_2(Mg,Cu)Cu_2[Si_2O_6]_2$	chain of edge-shared alternating CuO_4 and $(Mg,Cu)O_6$		108
$Cu_2(AsO_4)(OH) \cdot 3H_2O$, euchroite	octahedral chain cross-linked by AsO_4 through branched CuO_6 by sharing edges		109
$Cu(AsO_3OH)(H_2O)$, geminite	edge-shared zigzag octahedral chain		112
$Cu_3(Zn,Cu)_4Cd_2(AsO_4)_6(H_2O)_2$, keyite	vertex-shared octahedral chain		113
$Cu_3AsO_4(OH)_3$, clinoclase	chain of vertex-sharing trimers (2 edge-shared Cu_2O_8 + vertex-shared CuO_5)		115
$MCu_6(XO_4)_3(OH)_6 \cdot 3H_2O$, where M = Bi, Y, rare-earth element, Ca, Al; X = As, P; Ca-rich agardite	octahedral chain		116
β-$NaCuPO_4$	chain of alternating CuO_4 and CuO_6[4+2]	ferrimagnetic, T_c = 18 K	135, this work
$[Na_2Cu_3(PO_4)_2][CuOCl]$	chain of fused CuO_6 and CuO_4	antiferromagnetic	this work
$CuHPO_3 \cdot 2H_2O$	chain of distorted CuO_6		119
α-$NaCuPO_4$	chain of vertex-shared CuO_5[4+1]		120
β-$AgCuPO_4$	chain of edge-shared CuO_5[4+1]	T_N = 45 K	121
$Cu_2K(OH)(PO_3F)_2 \cdot H_2O$	chain of edge-shared CuO_6[4+2] octahedra		125
$[CuMg(PO_4)(OH)(H_2O)_2]_2(H_2O)$, nissonite	edge-shared CuO_6[4+2] octahedral chain		131
$Bi_2Cu_3(OH)_2O_2(PO_4)_2 \cdot 2H_2O$, mrazekite	edge-shared octahedral chains interlinked by vertex-shared CuO_6		134
$BaCu_2(PO_4)_2$	chains of vertex-shared square planar CuO_5	antiferromagnetic, a large maximum at 65 K	136
$BiCu_2PO_6$	double chains of vertex-sharing dimers of edge-shared CuO_5 square pyramids		137
$Cu_9O_2(PO_4)_4(OH)_2$	zigzag double chains of edge-shared CuO_4 and CuO_5		138
$Cu_3PO_4(OH)_3$, cornetite	chain of edge-shared dimers		139
$Cu_3(AsO_4)_2$-I	edge-sharing CuO_6[4+2] chain		147
	Sheets		
$KCu_3(OH)_2[(AsO_4)H(AsO_4)]$	CuO_6 octahedral sheet		98
$Cu_4(AsO_4)_2O$	CuO_5, square pyramidal and trigonal bipyramidal, layer	antiferromagnetic, 30−300 K	101
$Cu_5(SiO_3)_4(OH)_2$, shattuckite	$(CuO_2)_n$ layer, consisting distorted CuO_6 octahedra, interlinked by square planar CuO_4		102
$Cu_8(Si_4O_{11})_2(OH)_4 \cdot xH_2O$, planchéite	similar to that of shattuckite		102
$BaCu_2Si_2O_7$	vertex-sharing CuO_5[4+1] layer separated by Si_2O_7		106
$(Cu,Zn)_3Pb(AsO_4)_2(OH)_2$, bayldonite	edge-sharing CuO_6 octahedral sheet		114
$(Cu,Zn)_2ZnPO_4(OH)_3 \cdot 2H_2O$, veszelyite	edge-sharing CuO_6 octahedra		117
$Cu_5(PO_4)_2(OH)_4$, pseudomalachite	edge-sharing CuO_6[4+2] and CuO_5[4+1]		118
$Cu_3(PO_4)_2 \cdot H_2O$	vertex- and edge-shared CuO_6[4+2], CuO_5[4+1], and CuO_4[4]		123
$KCuPO_4$	sheet of vertex-shared CuO_5[4+1] square pyramids		133
$KCuPO_4 \cdot H_2O$	vertex-sharing CuO_5[4+1] sheet		142
$Cu_3(AsO_4)_2$-III	vertex- and edge-sharing CuO_n (n = 4,5)		99

Table 3 (Continued)

compound	special frameworks	property	ref
	Mixed Frameworks		
$Pb_2Cu^{II}_7(AsO_4)_6$	chains of vertex-, edge-shared CuO_4/CuO_5		96
$Pb_2Cu^{I}_2Cu^{II}_6(AsO_4)_6$	corrugated sheets of interconnected chains of vertex-, edge-shared CuO_4/CuO_5		96
$Ca_3Cu_5Si_9O_{26}$, liebauite	extended vertex-/edge-sharing CuOn (n = 5, 6)		91
$AgCu_4(AsO_4)_3$	edge-shared CuO_n (n = 4, 6)		94
$NaCu_4(AsO_4)_3$	edge-shared CuO_n (n = 4, 6)		95
$KCu_4(AsO_4)_3$	edge-shared CuO_n (n = 4, 6)		99
$Cu_6[Si_6O_{18}]\cdot 6H_2O$, dioptase	corner-linked nearly planar Cu_2O_6 dimers formed by pairs of edge-shared CuO_4	antiferromagnetic, $T_N = \sim 70$ K	104, 105
Cu_2PO_4	vertex-shared $Cu^{II}O_6$, $Cu^{II}O_5$, and $Cu^{I}O_2$	antiferromagnetic	this work
$KCu_4(PO_4)_3$	edge-shared CuO_5[4+1] square pyramids and CuO_5 trigonal pyramids		126
$Cu_6(Si_6O_{18})\cdot 6H_2O$	edge-sharing CuO_6[4+2]		143
$Cu_2AsO_4(OH)$, olivenite	vertex- and edge-sharing CuO_n (n = 5,6)		145
$Cu_3(AsO_4)_2$-II	vertex- and edge-sharing CuO_n (n = 4−6)		146

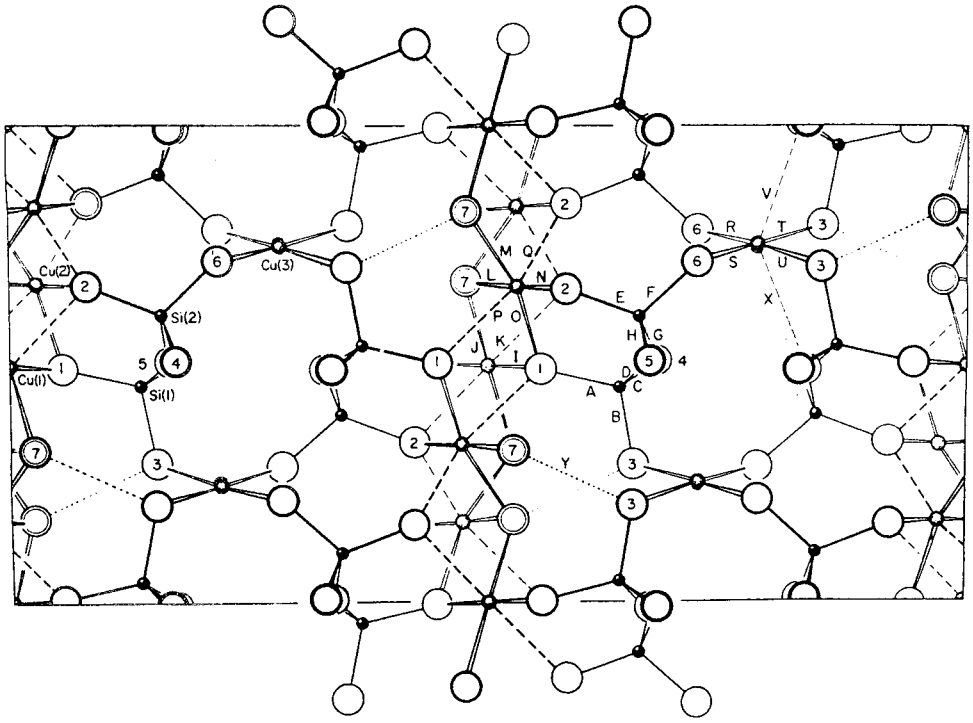

Figure 9. Plan of the unit cell of the crystal structure of shattuckite, $Cu_5(SiO_3)_4(OH)_2$, viewed along the *c* axis (*b* axis is horizontal). In the distorted octahedral Cu coordination, the longer apical bonds are dashed. Hydrogen bonds are dotted. Large, double circles represent OH groups. (Reprinted with permission from ref 102.)

surrounded by the closed-shell anions SO_4^{2-} and SiO_4^{4-} and "shield" from each other further by Pb^{2+} cations. Judging from the structure, wherryite should be a good example for the study of magnetic interactions in the confined one-dimensional Cu−O chain.

A new bismuth copper(II) oxyphosphate, $BiCu_2PO_6$, that exhibits a novel double Cu−O chain has been synthesized recently.[137] The double chain, as shown in Figure 12, is composed of vertex-shared dimeric units Cu_2O_8 made of edge-shared CuO_5 square pyramids. The CuO_5 is [4 + 1] coordinate, forming four short (1.94−2.02 Å) and one long (2.19 Å) distance. The double chain is connected to edge-shared BiO_5 pyramidal chains to constitute sheets parallel to the (100) plane. The sheets are connected through the PO_4 tetrahedra. Again, no magnetic properties have been investigated.

In the past 5 years, we have been looking into copper-containing silicate, phosphate, and arsenate systems because of interest in low-dimensional copper oxides. It should be noted that, although a large collection of copper-containing compounds were reported prior to this study, recent discoveries have revealed that an abundant chemistry featuring low-dimensional, copper oxide structures is yet to come. This is attributed in part to the different reaction medium provided by molten-salt synthesis, compared to the traditional solid-state and hydrothermal methods used for the previous studies. The first three of the following four novel compounds, $Li_2Cu_3Si_4O_{12}$,[148] $ANa_5Cu_4(AsO_4)_4Cl_2$ (A = Rb, Cs),[149,150] β-$NaCuPO_4$,[135,148] and $LiCu_2PO_5$,[148] containing different nanometer-size Cu−O frameworks, trimetal-, tetrametal-center units, pseudo-one-dimensional chain, and double-layer slab structures, respectively, are discussed below.

The attractive trimeric $[Cu_3O_8]^{10-}$ and tetrameric $[Cu_4O_{12}]^{16-}$ (Figure 13) units are identified in otherwise structurally complicated $Li_2Cu_3Si_4O_{12}$ and $CsNa_5Cu_4(AsO_4)_4Cl_2$ lattices, respectively. It is recognized that these "oligomeric" Cu−O structural units are uniformly distributed in the extended lattice, i.e. each

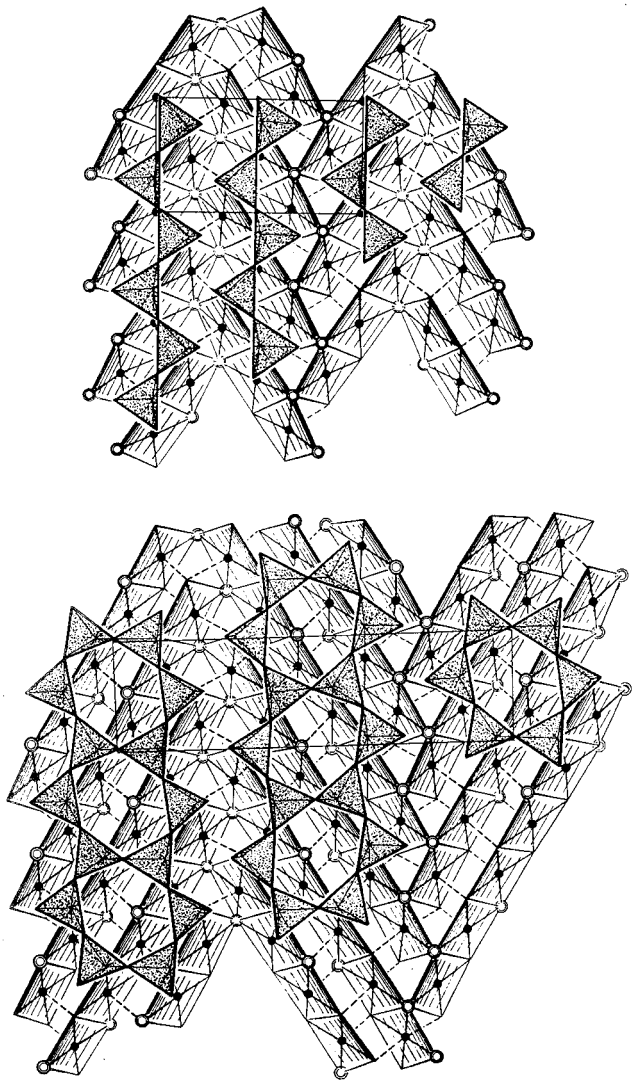

Figure 10. Schematic views of the triple layers in shattuckite (top) and planchéite (bottom), viewed along the *b* axis. The rows of planar CuO_4 groups are shown as crossed squares. The longer apical Cu−O bonds are dashed. The double circles represent OH groups. (Reprinted with permission from ref 102.)

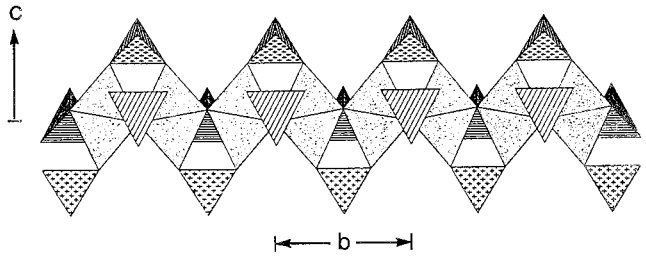

Figure 11. The CuO_6 octahedral chain (randomly dotted) in wherryite viewed down [100]. (SO_4) tetrahedra are cross-shaded, and (SiO_4) tetrahedra are line-shaded. (Reprinted with permission from ref 107.)

framework possesses an exclusive structure unit of nanosized copper(II) oxide. These structural units are well-separated from each other by the oxyanion spacer. The closest Cu−Cu distance between neighboring fragments is not less than 5.00 Å. This distance, in fact, is far longer than 2.56 Å in elemental copper.[151]

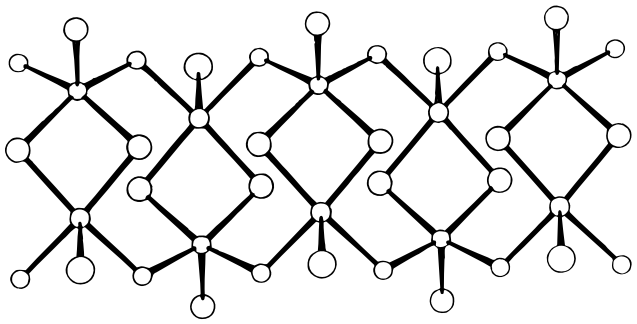

Figure 12. The copper double chain running along the *b* axis. (Reprinted with permission from ref 137.)

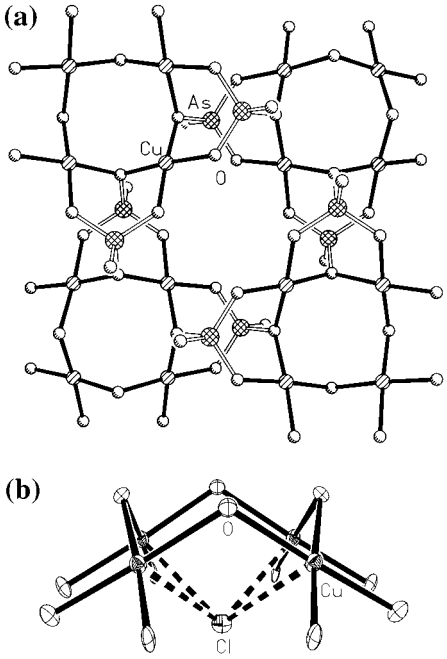

Figure 13. (a) Arrangment of the condensed $[Cu_4O_{12}]^{16-}$ tetramers and $[AsO_4]^{3-}$ units in the Cu−As−O sheet. Mirror planes are present across the opposite bridging oxygen atoms of the Cu_4O_4 core. (b) Structure of the crown-like $[Cu_4O_{12}]^{16-}$ tetramer capped with the Cl^- anion (70% thermal ellipsoids).

The Cu_4O_{12} cluster adopts an interesting cyclo-S_8-like Cu_4O_4 core (Figure 13b). This puckered geometry is attributed to the bond strength of the fused $[AsO_4]$ units and the steric effect of the capping Cl^- anion. The copper atoms lie in a plane between the layers of the nearly planar arrays of bridging oxygen atoms (O^b), two O(2) and two O(4), and terminal oxygen atoms (O^t), four O(5) and four O(6). The four Cu−O bond distances of the Jahn−Teller $[CuO_4]$ unit are in a narrow range, 1.93−1.99 Å, where the shorter bonds correspond to O^t and the longer bonds correspond to O^b. The sum of the four O−Cu−O angles is 359.7°, indicating that the $[CuO_4]$ unit adopts a nearly square planar configuration. The Cu−Cl distance from the capping Cl(1) to the Cu_4 square, 2.73 Å, is long compared with the sum of Shannon crystal radii, 2.46 Å, for a 5-coordinate Cu^{2+} cation (0.79 Å) and a 6-coordinate Cl^- (1.67 Å).[152]

A remarkable similarity in general structural features is evident between the Cu_4O_4 core of the cluster and the building block found in the puckered Cu−O layer of the high-T_c cuprate superconductors.[3] With respect to high-T_c superconductivity, it is well-known that the Cu−O layers are considered critical structural features.

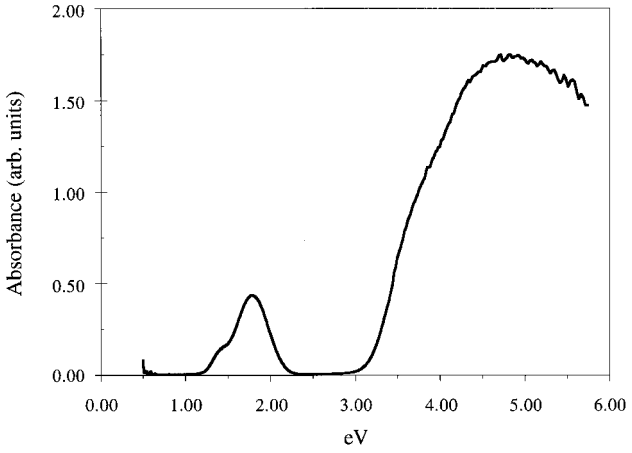

Figure 14. Optical absorption spectrum of $CsNa_5Cu_4(AsO_4)_4Cl_2$.

A brief comparison of the Cu_4O_{12} cluster in this compound with the CuO_2 layers in the $YBa_2Cu_3O_{7-\delta}$ structure shows that the in-plane $Cu^{II}-O$ distances are comparable, 1.94 Å for $YBa_2Cu_3O_{7-\delta}$ vs 1.96 Å for the average distance in the Cu_4O_{12} cluster. The thickness of the puckered CuO_2 layer is 0.27 Å, however, as opposed to 1.09 Å with respect to the Cu_4O_4 core. The highly puckered Cu_4O_{12} unit containing Cu−O−Cu angles (mean value 109.5°) are much different than those found in $YBa_2Cu_3O_{7-\delta}$ (distorted linear ca. 165°). Consequently, the Cu−Cu distances along the edge of the Cu_4 square are shorter, ca. 3.22−3.24 Å vs 3.82−3.89 Å, respectively.

The electronic absorption spectrum was recorded in the range 0.50−6.20 eV (Figure 14). Based on a preliminary analysis of the spectrum, the intense absorptions above 24 000 cm^{-1} can be assigned to LMCT bands from the σ lone pair of the anions to the σ orbital of the copper, as similar assignments have been made in other Cu(II) complexes.[153] The specific assignment of bands is difficult because of multiple ligand interactions due to AsO_4^{3-} and Cl^- anions. The ligand-field spectra show broad bands, with maxima at 1.43 and 1.77 eV. While it is necessary to assign the bands with the assistance of an accurate electronic structure, the observed bands are in the region where the d-d transitions are generally observed.[153]

The variable-temperature magnetic susceptibility data of $CsNa_5Cu_4(AsO_4)_4Cl_2$ are plotted in Figure 15. The Curie−Weiss fit of the χ^{-1} curve in the 150−300 K region results in a negative Weiss constant, $\theta = -36.5$ K, which is intrinsic to the antiferromagnetic (AF) coupling. The effective magnetic moment, $\mu_{eff} = 3.22\mu_B$, is comparable with the spin-only value. The χ^{-1} vs T curve shows a minimum at ∼50 K and a maximum at 11 K, typical for a dominant antiferromagnetic exchange interaction with some remaining paramagnetism (≅11 K). Detailed analysis is underway.

A fruitful structural chemistry arises from the versatile nature of bond interactions between distorted (Jahn−Teller) $Cu^{II}O_{6-x}$ ($x = 0-2$) polyhedra and tetrahedral oxy groups. The previously reported β-$NaCuPO_4$ exhibits a pseudo-one-dimensional Cu−O chain.[135,148] It is also worth noting that, in each structural unit, there are two different crystallographic Cu(II) sites whose CuO_x ($x = 4-6$) coordination is suitable for accommodating trivalent copper, Cu(III). Chemical substitution of Si^{4+} for P^{5+} in this known compound, for example, will allow investigation of the magnetochemistry of $NaCuP_{1-x}Si_xO_4$ as a function of x. The preliminary examination of β-$NaCuPO_4$ reveals unusual low-temperature magnetic properties. The χ^{-1} vs T curve indicates that the magnetic behavior obeys the Curie−Weiss Law at temperatures in the range of 20−300 K with a ferromagnetic transition occurring at around 18 K (Figure 16a). The field-dependent magnetization plots (Figure 16b) show a rapid increase in M at temperatures below the transition, as opposed to a constant M above the transition point. It is noted that similarly interesting magnetic behavior has been ob-

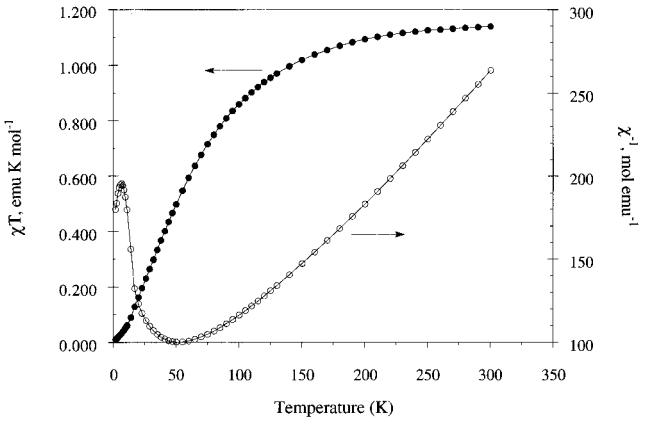

Figure 15. The magnetic susceptibility data of $CsNa_5Cu_4(AsO_4)_4Cl_2$ are plotted as *both* χ vs T (solid dots) and inverse molar susceptibility (χ^{-1}, open circles) vs temperature (T).

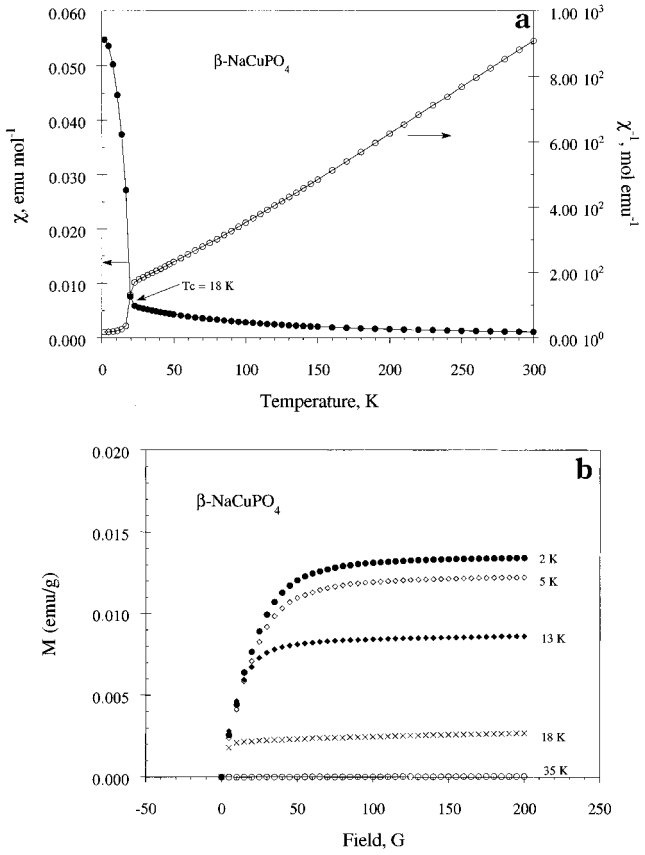

Figure 16. (a) The magnetic susceptibility and (b) the field-dependent magnetization plots of β-$NaCuPO_4$.

served in other low-dimensional solid-state materials.[154]

Brief investigations into the mixed-valence copper(I/II) compounds has shown complex structural formation, e.g., Cu_2PO_4[155] and $Na_2Cu_4(PO_4)_2Cl$.[156] The latter can be reformulated as $[Na_2Cu^{II}_3(PO_4)_2][Cu^{I}OCl]$. The $Cu^{II}-O$ units form linear chains made of fused $[CuO_6]$ and $[CuO_4]$ polyhedra and bridged to the $Cu^{I}-O$ chain by the electronegative anion, Cl^-. The closely spaced Cu^{2+} magnetic centers are bridged by oxo anions, giving rise to a possible competitive coupling between antiferro- and ferromagnetic ordering starting at ~220 K. The pseudo-binary compound Cu_2PO_4 has an attractive extended framework which consists of low-dimensional arrays of nearly parallel $Cu^{I}O_2$ linear units and short Cu^{I}-$O-Cu^{II}-O-Cu^{I}$ and $Cu^{II}-O-Cu^{II}$ linkages. The $Cu^{I}O_2$ units are closely spaced, at 2.74 Å, due to cross-linking via the PO_4 tetrahedra. The magnetic data shows a broad transition to antiferromagnetic ordering below 170 K.

Conclusions and Future Directions

This review has abstracted a large family of transition-metal oxide containing silicates, phosphates, and arsenates with respect to the framework of TM oxide layers, chains, and oligomers. In studying this class of solids, we have come to realize that the lattice confinement may be accomplished chemically by chelation with closed-shell, nonmagnetic oxyanions (XO_x^{n-}, X = Si, P, As). The chemically dissimilar higher nuclearity molecular complexes briefly discussed in this review demonstrate the same feasibility of using organic-based, closed-shell ligands to achieve structural isolation and electronic insulation of TM oxide-based magnetic clusters. For comparative studies, one should also consider in these studies the inorganic/organic hybrid materials where structurally confined TM oxide frameworks have been observed.[157]

Structurally confined TM oxide frameworks that exist in molecular complexes and extended solids adopt a large variety of geometries. Intuitively, the magnetic properties are going to be diverse. To systematically study these compounds will lead to a larger database with respect to the correlation between magnetic coupling and confined lattice,[158] and it is potentially important for the continued development of a fundamental understanding of the magnetochemistry of TM-based oxide materials.

The accumulated synthetic expertise on Ti-, Mn-, Cu-based silicates, phosphates, and arsenates can now be channeled into additional areas. The high-oxidation state, middle transition-metal as well as other oxyanion systems, such as borates and aluminates, are immediate candidates. Some preliminary work has been started in our research group. Given the variety and fundamental importance of the magnetochemistry, the greater materials database promises to deliver would make the invested time and effort well worthwhile.

Acknowledgment. Financial support for this research (DMR-9612148), the single crystal X-ray diffractometer (CHE-9207230), and magnetometer (CHE-9414402) from the National Science Foundation is gratefully acknowledged. The author also gives special thanks to the coauthors listed in the publications, especially K. M. S. Etheredge, Q. Huang, D. L. Serra, S. Wang, and T. A. Wardojo, for their important contributions and insight.

References

(1) Bednorz, G.; Müller, K. A. *Z. Phys. B.* **1986**, *64*, 189−193.
(2) (a) Wu, M. K.; Ashburn, J. R.; Throng, C. J.; Hor, P. H.; Meng, R. L.; Gao, L.; Huang, Z. J.; Wang, Y. Q.; Chu, C. W. *Phys. Rev. Lett.* **1987**, *58*, 908−910. (b) Hor, P. H.; Gao, L.; Meng, R. L.; Huang, Z. J.; Wang, Y. Q.; Forster, K.; Vassiliou, J.; Chu, C. W.; Wu, M. K.; Ashburn, J. R.; Thong, C. J. *Phys. Rev. Lett.* **1987**, *58*, 911−912.
(3) (a) Raveau, B.; Michel, C.; Hervieu, M.; Groult, D. *Springer Series in Materials Science 15, Crystal Chemistry of High T_c Superconducting Oxides*; Springer-Verlag: New York, 1991. (b) Anderson, M. T.; Vaughey, J. T.; Poeppelmeier, K. R. *Chem. Mater.* **1993**, *5*, 151−165. (c) Park, C.; Synder, R. L. *J. Am. Ceram. Soc.* **1995**, *78*, 3171−3139 and review articles cited therein.
(4) Gunther, L. *Phys. World* **1990**, *3*, 28−34.
(5) Dagani, R. *Chem. Eng. News* **1992**, *70*, 18−24.
(6) Awschalom, D. D.; DiVincenzo, D. P.; Smyth, J. F. *Science* **1992**, *258*, 414−421.
(7) Miller, J. S.; Epstein, A. J. *Angew. Chem., Int. Ed. Engl.* **1994**, *33*, 385−415.
(8) *Phase Diagrams for Ceramists;* The American Ceramic Society, Inc.: Westerville, OH, Vols. 1−V.
(9) (a) [BaCl][$CuPO_4$]: Etheredge, K. M. S.; Hwu, S.-J. *Inorg. Chem.* **1995**, *34*, 3123−3125. (b) [$Na_2Cu_2(PO)_2$][CuOCl]: Etheredge K. M. S.; Hwu, S.-J. *Inorg. Chem.* **1996**, *35*, 5278−5282. (c) $Ba_3CuBr_3(P_2O_7)$: Etheredge, K. M. S.; Mackay, R.; Schimek, G. L.; Hwu, S.-J. *Inorg. Chem.* **1996**, ***35***, 7919−7921.
(10) Nakua, A. M.; Greedan, J. E. *J. Solid State Chem.* **1995**, *118*, 402−411.
(11) Wang, S.; Hwu, S.-J. *J. Solid State Chem.* **1991**, *90*, 31−41.
(12) Wang, S., Ph.D. Dissertation, Rice University, 1993.
(13) (a) Ballhausen, C. J. *Introduction to Ligand Field Theory*; McGraw-Hill Book Company, Inc.: New York, 1962; pp 226−292. (b) Harrison, W. T. A.; Liang, C. S.; Nenoff, T. M.; Stucky, G. D. *J. Solid State Chem.* **1994**, *113*, 376−381. (c) Ulutagay, M.; Schimek, G. L.; Hwu, S.-J.; Taye, H. *Inorg. Chem.* **1998**, *37*, 1507−1512.
(14) Caneschi, A.; Gatteschi, D.; Sessoli, R.; Rey, P. *Acc. Chem. Res.* **1989**, *22*, 392−398.
(15) El Fallah, M. S.; Rentschler, E.; Caneschi, A.; Sessoli, R.; Gatteschi, D. *Inorg. Chem.* **1996**, *35*, 3723−3724.
(16) Rentschler, E.; Gatteschi, D.; Cornia, A.; Fabretti, A. C.; Barra, A.-L.; Shchegolikhina, O. I.; Zhdanov, A. A. *Inorg. Chem.* **1996**, *35*, 4427−4431.
(17) Conia, A.; Fabretti, A. C.; Gatteschi, D.; Pályi, G.; Rentschler, E.; Shchegolikhina, O. I.; Zhdanov, A. A. *Inorg. Chem.* **1995**, *34*, 5383−5387.
(18) De Munno, G.; Julve, M.; Lloret, F.; Faus, J.; Verdaguer, M.; Caneschi, A. *Inorg. Chem.* **1995**, *34*, 157−165.
(19) Hatfield, W. E. *J. Appl. Phys.* **1981**, *52*, 1985−1990.
(20) Stamp, P. C. E.; Chudnosvsky, E. M.; Barbara, B. *Int. J. Mod. Phys.* **1992**, *B6*, 1355.
(21) Michael, R. D.; Shull, R. D.; Swartzendruber, L. J.; Bennett, L. H.; Watson, R. E. *J. Magn. Magn. Mater.* **1992**, *111*, 29−33.
(22) Miller, J. S.; Epstein, A. J. *Angew. Chem., Int. Ed. Engl.* **1994**, *33*, 385−415.
(23) Christou, G. *Acc. Chem. Res.* **1989**, *22*, 328−335 and references therein.
(24) Li, Q.; Vincent, J. B.; Libby, E.; Chang, H.-R.; Huffman, J. C.; Boyd, P. D. W.; Christou, G.; Hendrickson, D. N. *Angew. Chem., Int. Ed. Engl.* **1988**, *27*, 1731−1733.
(25) Boyd, P. D. W.; Li, Q.; Vincent, J. B.; Folting, K.; Chang, H.-R.; Streib, W. E.; Huffman, J. C.; Christou, G.; Hendrickson, D. N. *J. Am. Chem. Soc.* **1988**, *110*, 8537−8539**.**
(26) Eppley, H. J.; Aubin, S. M. J.; Streib, W. E.; Bollinger, J. C.; Hendrickson, D. N.; Christou, G. *Inorg. Chem.* **1997**, *36*, 109−115.
(27) Wang, S.; Tsai, H.-L.; Streib, W. E.; Christou, G.; Hendrickson, D. N. *J. Chem. Soc., Chem. Commun.* **1992**, 677−679.
(28) Wemple, M W.; Tsai, H.-L.; Streib, W. E.; Hendrickson, D. N.; Christou, G. *J. Chem. Soc., Chem. Commun.* **1994**, 1031−1033.
(29) Christmas, C.; Vincent, J. B.; Chang, H.-R.; Huffman, J. C.; Christou, G.; Hendrickson, D. N. *J. Am. Chem. Soc.* **1988**, *110*, 823−830.
(30) Low, D. W.; Eichhorn, D. M.; Draganescu, A.; Armstrong, W. H. *Inorg. Chem.* **1991**, *30*, 877−878.
(31) Hagen, K. S.; Armstrong, W. H. *J. Am. Chem. Soc.* **1989**, *111*, 774−775.
(32) Wadsley, A. D. *Acta Crystallogr.* **1955**, *8*, 165−172.
(33) Wells, A. F. *Structural Inorganic Chemistry*, 5th ed.; Clarendon Press: Oxford, 1984; pp 553−556.

(34) Wadsley, A. D. *Acta Crystallogr.* **1952**, *5*, 676−680.
(35) Goldberg, D. P.; Caneschi, A.; Lippard, S. J. *J. Am. Chem. Soc.* **1993**, *115*, 9299−9300.
(36) Cavaluzzo, M.; Chen, Q.; Zubieta, J. *J. Chem. Soc., Chem. Commun.* **1993**, 131−133.
(37) (a) Squire, R. C.; Aubin, S. M. J.; Folting, K.; Streib, W. E.; Hendrickson, D. N.; Christou, G. *Angew. Chem., Int. Ed. Engl.* **1995**, *34*, 887−889. (b) Squire, R. C.; Aubin, S. M. J.; Folting, K.; Streib, W. E.; Christou, G.; Hendrickson, D. N. *Inorg. Chem.* **1995**, *34*, 6463−6471.
(38) Tsai, H.-L.; Eppley, H. J.; de Vries, N.; Folting K.; Christou, G.; Hendrickson, D. N. *J. Chem. Soc., Chem. Commun.* **1994**, 1745−1746.
(39) Luneau, D.; Savariault, J.-M.; Tuchagues, J.-P. *Inorg. Chem.* **1988**, *27*, 3912−3918.
(40) Sun, Z.; Gantzel, P. K.; Hendrickson, D. N. *Inorg. Chem.* **1996**, *35*, 6640−6641.
(41) Tsai, H.-L.; Wang, S.; Folting, K.; Streib, W. E.; Hendrickson, D. N.; Christou, G. *J. Am. Chem. Soc.* **1995**, *117*, 2503−2513.
(42) Sessoli, R.; Tsai, H.-L.; Schake, A. R.; Wang, S.; Vincent, J. B.; Folting, K.; Gatteschi, D.; Christou, G.; Hendrickson, D. N. *J. Am. Chem. Soc.* **1993**, *115*, 1804−1816.
(43) Eppley, H. J.; Tsai, H.-L.; de Vries, N.; Folting, K.; Christou, G.; Hendrickson, D. N. *J. Am. Chem. Soc.* **1995**, *117*, 301−317.
(44) Lis, T. *Acta Crystallogr.* **1980**, *B36*, 2042−2046.
(45) Goldberg, D. P.; Caneschi, A.; Delfs, C. D.; Sessoli, R.; Lippard, S. J. *J. Am. Chem. Soc.* **1995**, *117*, 5789−5800.
(46) Gorun, S. M.; Stribrany, R. T. U.S. Patent 5,041,575, 1991.
(47) ICSD: *Inorganic Crystal Structure Database*, Gmelin-Institut für Anorganische Chemie and Fachinformationszentrum FIZ Karlsruhe.
(48) (a) Wang, S.; Hwu, S.-J. *J. Am. Chem. Soc.* **1992**, *114*, 6920−6922. (b) Chen, S. C.; Ramanujachary, K. V.; Greenblatt, M. *Inorg. Chem.* **1994**, *33*, 5994−5998. (c) Wang, S.; Hwu, S.-J. *Inorg. Chem.* **1995**, *34*, 166−171. (d) Wang, S.; Hwu, S.-J.; Paradis, J. A.; Whangbo, M.-H. *J. Am. Chem. Soc.* **1995**, *117*, 5515−5522. (e) Gueho, C.; Giaquinta, D.; Mansot, J. L.; Ebel, T.; Palvadeau, P. *Chem. Mater.* **1995**, *7*, 486-492.
(49) Wells, A. F. *Structural Inorganic Chemistry*; 5th ed., Oxford University Press: New York, 1984; p 540.
(50) Visser, D.; Carling S. G.; Day, P.; Deportes, J. *J. Appl. Phys.* **1991**, *69*, 6016−6018.
(51) Liao, J.-H.; Leroux, F.; Guyomard, D.; Piffard, Y.; Tournoux, M. *Eur. J. Solid State Inorg. Chem.* **1995**, *32*, 403−414.
(52) Adams, R. D.; Layland R.; Payen, C. *Polyhedron* **1995**, *14*, 3473−3480.
(53) Huang, Q.; Hwu, S.-J. *Inorg. Chem.* **1998**, in press.
(54) (a) Armbruster, T.; Oberhänsli, R.; Kunz, M. *Am. Mineral.* **1993**, *78*, 1088−1095. (b) Moore, P. B.; Araki, T. *Z. Kristallogr.* **1979**, *150*, 287−297.
(55) Tyrna, P. L.; Guggenheim, S. *Am. Mineral.* **1991**, *76*, 266−271.
(56) Klaska, K. H.; Jarchow, O. *Z. Kristallogr.* **1977**, *145*, 46−65.
(57) Leroux, F.; Mar, A.; Payen, C.; Guyomard, D.; Verbaere, A.; Piffard, Y. *J. Solid State Chem.* **1995**, *115*, 240−246.
(58) (a) Moore, P. B.; Araki, T. *Am. Mineral.* **1976**, *61*, 1226−1240. (b) Moore, P. B.; Araki, T. *Inorg. Chem.* **1977**, *16*, 1839−1847. (c) Moore, P. B.; Shen, J.; Araki, T. *Am. Mineral.* **1985**, *70*, 171−181.
(59) Wan C.; Ghose, S. *Am. Mineral.* **1978**, *63*, 3−571.
(60) (a) Peacor, D. R.; Niizeki, N. *Z. Kristallogr.* **1963**, *119*, 98−116. (b) Ohashi, Y.; Finger, L. W. *Carnegie Inst. Wash. Year Book*, **1975**, *74*, 564−569.
(61) de Villiers, J. P. R. *Am. Mineral.* **1980**, *65*, 756−765.
(62) Lightfoot, P.; Cheetham, A. K.; Slight, A. W. **1988**, *73*, 325−329.
(63) Moore, P. B. *Am. Mineral.* **1967**, *52*, 1603−1613.
(64) Lightfoot, P.; Cheetham, A. K. *J. Solid State Chem.* **1989**, *78*, 17−22.
(65) Moore, P. B. *Am. Mineral.* **1970**, *55*, 1489−1499.
(66) Narita, H.; Koto, K.; Morimoto, N. *Acta Crystallogr.* **1975**, *B31*, 2422−2426.
(67) Ohashi, H.; Osawa, T.; Tsukimura, K. *Acta Crystallogr.* **1987**, *C43*, 605−607.
(68) ICSD-31864: Gabrielson, O. *Arkiv Mineral. Geol.* **1962**, *3*, 141−151.
(69) ICSD-100478: Basso, R.; della Giusta, A. *Neues Jahrbuch fuer Mineral.. Abhandlungen (Band-Nr)* **1980**, *138*, 332−342.
(70) ICSD-200702: Catti, M., Chiari, G.; Ferraris, G. *Bull. Mineral.* **1980**, *103*, 129−134.
(71) ICSD-36273: Moore, P. B. *Arkiv Mineralogi Geologi* **1969**, *4*, 459−466.
(72) ICSD-15754: Bystroem A.; Mason, B. *Arkiv. Kemi, Mineral. Geol.* **1943**, *16*, 1−8.
(73) ICSD-20480: Astakhova, L. P.; Pobedimskaya, E. A.; Simonov, V. I. *Doklady, Akad. Nauk SSSR* **1967**, *173*, 1401−1403.
(74) ICSD-20637: Mamedov, H. S. *Doklady Akad. Nauk Azerbaidzhanskoi SSR* **1958**, *14*, 445−450.
(75) ICSD-200162: Simonov, M. A.; Belokoneva, E. L.; Egorov-Tismenko, Y. K.; Belov, N. V. *Doklady Akad. Nauk SSSR* **1977**, *234*, 586−589.
(76) ICSD-200167: Sandomirskii, P. A.; Simonov, M. A., Belov, N. V. *Doklady Akad. Nauk SSSR* **1977**, *233*, 1090−1093.
(77) ICSD-20121: Pushcharovskii, D. Y.; Pobedimskaya, E. A.; Belov, N. V. *Doklady Akad. Nauk SSSR* **1969**, *185*, 1045−1048.
(78) ICSD-20111: Pushcharovskii, D. Y.; Pobedimskaya, E. A.; Litvin, B. N.; Belov, N. V. *Doklady Akad. Nauk SSSR* **1974**, *214*, 91−94.
(79) ICSD-38210: Bjoerling, C. O.; Westgren, A. *Geol. Foereningens I Stockholm Foerhandlingar* **1938**, *60*, 67−72.
(80) ICSD-71814: Aranda, M. G.; Attfield, J. P.; Bruque, S. *Mater. Sci. Forum* **1991**, *79*, 827−832.
(81) ICSD-62287: Yakubovich, O. V.; Evdokimova, O. A.; Mel′nikov, O. K.; Simonov, M. A. *Kristallografiya* **1986**, *31*, 258−263.
(82) ICSD-39678: Yakubovich, O. V.; Mel′nikov, O. K. *Kristallografiya* **1993**, *38*, 58−62.
(83) ICSD-71465: Armbruster, T.; Oberhaensli, R.; Bermanec, V. *Eur. J. Mineral.* **1992**, *4*, 17−22.
(84) ICSD-39401: Rastsvetaeva, R. K.; Tamazyan, R. A.; Sokolova, E. V.; Belakovskii, D. I. *Kristallografiya* **1991**, *36*, 354−360.
(85) ICSD-25793: Morimoto, N.; Koto; Shinohara, T. *Mineral. J. (Jpn.)* **1966**, *5*, 44−64.
(86) Moring, J.; Kostiner, E. *J. Solid State Chem.* **1986**, *61*, 379−383.
(87) Geller, S.; Durand, J. L. *Acta Crystallogr.* **1960**, *13*, 325−331.
(88) Kawamura, K.; Kawahara, A. *Acta Crystallogr.* **1976**, *B32*, 2419−2422.
(89) Kawamura, K.; Kawahara, A.; Iiyama, J. T. *Acta Crystallogr.* **1978**, *B34*, 3181−3185.
(90) Heinrich, A.; Gramlich, V. *Naturwissenschaften* **1982**, *69*, 142−143.
(91) Zöller, M. H.; Tillmanns, E. *Z. Kristallogr.* **1992**, *200*, 115−126.
(92) Janczak, J.; Kubiak, R. *Acta Crystallogr.* **1992**, *C48*, 8−10.
(93) Watanabe, I.; Kawahara, A. *Acta Crystallogr.* **1993**, *C49*, 854−856.
(94) Riffel, H.; Keller, P.; Hess, H. *Z. Anorg. Allg. Chem.* **1985**, *530*, 60−68.
(95) Pertlik, F. *Acta Crystallogr.* **1987**, *C43*, 381−383.
(96) Effenberger, H. *J. Solid State Chem.* **1995**, *114*, 413−419.
(97) Effenberger, H.; Pertlik, F. *J. Solid State Chem.* **1987**, *70*, 219−224.
(98) Effenberger, H. *Z. Kristallogr.* **1989**, *188*, 43−56.
(99) Effenberger, H. *Monatsh. Chem.* **1988**, *119*, 1103−1112.
(100) Osterloh, D.; Müller-Buschbaum, Hk. *Z. Anorg. Allg. Chem.* **1994**, *620*, 651−654.
(101) Adams, R. D.; Layland, R.; Payen, C. *Inorg. Chem.* **1995**, *34*, 5397−5398.
(102) Evans, H. T., Jr.; Mrose, M. E. *Am. Mineral.* **1977**, *62*, 491−502.
(103) Moqine, A.; Boukhari, A.; Darriet, J. *J. Solid State Chem.* **1993**, *107*, 362−367.
(104) Ribbe, P. H.; Gibbs, G. V.; Hamil, M. M. *Am. Mineral.* **1977**, *62*, 807−811.
(105) Newnham, R. E.; Santoro, R. P. *Phys. status solidi* **1967**, *19*, K87−90.
(106) Janczak, J.; Kubiak, R. *Acta Crystallogr.* **1990**, *C46*, 1383−1385.
(107) Cooper, M.; Hawthorne, F. C. *Canadian Mineralogist* **1994**, *32*, 373−380.
(108) Horiuchi, H.; Saito, A.; Tachi, T.; Nagasawa, H. *Am. Mineral.* **1997**, *82*, 143−148.
(109) Boudjada, A.; Masse, R.; Guitel, J. C. *Acta Crystallogr.* **1982**, *B38*, 710−713.
(110) (a) Finney, J. J. *Acta Crystallogra.* **1966**, *21*, 437−440. (b) Eby, R. K.; Hawthorne, F. C. *Acta Crystallogr.* **1989**, *C45*, 1479−1482.
(111) (a) Kolesova, R. V.; Fesenko, E. G. *Sov. Phys. Crystallogr.* **1968**, *13*, 324−328. (b) Burns, P. C.; Eby, R. K.; Hawthorne, F. C. *Acta Crystallogr.* **1991**, *C47*, 916−919.
(112) Cooper, M. A.; Hawthorne, F. C. *Canadian Mineralogist* **1995**, *33*, 1111−1118.
(113) Ghose, S.; Wan, C. *Acta Crystallogra.* **1979**, *B35*, 819−823.
(114) Cooper, M. A.; Hawthorne, F. C. *Canadian Mineralogist* **1996**, *34*, 623−630.
(115) (a) Ghose, S.; Fehlmann, M.; Sundaralingam, M. *Acta Crystallogr.* **1965**, *18*, 777−787. (b) Eby, R. K.; Hawthorne, F. C. *Acta Crystallogr.* **1990**, *C46*, 2291−2294.
(116) Aruga, A.; Nakai, I. *Acta Crystallogr.* **1985**, *C41*, 161−163.
(117) Ghose, S.; Leo, S. R.; Wan, C. *Am. Mineral.* **1974**, *59*, 573−581.
(118) (a) Ghose, S. *Acta Crystallogr.* **1963**, *16*, 124−128. (b) Shoemaker, G. L.; Anderson, J. B.; Kostiner, E. *Am. Mineral.* **1977**, *62*, 1042−1048. (c) Anderson, J. B.; Shoemaker, G. L.; Kostiner, E.; Ruszala, F. A. *Am. Mineral.* **1977**, *62*, 115−121. (d) Shoemaker, G. L.; Anderson, J. B.; Kostiner, E. *Am. Mineral.* **1981**, *66*, 169−175.
(119) Handlovic, M. *Acta Crystallogr.* **1969**, *B25*, 227−231.
(120) Quarton, P. M. *Acta Crystallogr.* **1983**, *C39*, 664−667.
(121) Quarton, M.; Oumba, M. T. *Mater. Res. Bull.* **1983**, *18*, 967−974.

(122) Shoemaker, G. L.; Kostiner, E.; Anderson, J. B. *Z. Kristallogr.* **1980**, *152*, 317−332.
(123) Effenberger, H. *J. Solid State Chem.* **1985**, *57*, 240−247.
(124) Effenberger, H. *Z. Kristallogr.* **1985**, *172*, 97−104.
(125) Möwius, F.; Ziemer, B.; Reck, G.; Meisel, R. M.; Grunze, H. *Z. Anorg. Allg. Chem.* **1987**, *547*, 75−82.
(126) Effenberger, H. *Z. Kristallogr.* **1987**, *180*, 43−50.
(127) Averbuch-Pouchot, M. T. *Acta Crystallogr.* **1989**, *C45*, 1275−1277.
(128) Effenberger, H.; Pertlik, F. *Z. Kristallogr.* **1991**, *194*, 207−219.
(129) Sghyar, M.; Durand, J.; Cot, L.; Rafiq, M. *Acta Crystallogr.* **1990**, *C46*, 1378−1381.
(130) Zeibig, M.; Wallis, B.; Möwius, F.; Meisel, M. *Z. Anorg. Allg. Chem.* **1991**, *600*, 231−238.
(131) Groat, L. A.; Hawthorne, F. C. *Am. Mineral.* **1990**, *75*, 1170−1175.
(132) Moqine, A.; Boukhari, A. *Acta Crystallogr.* **1991**, *C47*, 2294−2297.
(133) Effenberger, H. *Z. Kristallogr.* **1984**, *168*, 113−119.
(134) (a) Ridkosil, T.; Srein, V.; Fabry, J.; Hybler, J.; Maximov, B. A. *Canadian Mineralogist* **1992**, *30*, 215−224. (b) Effenberger, H.; Krause, W.; Belendorff, K.; Bernhardt, H.-J.; Medenbach, O.; Hybler, J.; Petricek, V. *Canadian Mineralogist* **1994**, *32*, 365−372.
(135) Kawahara, A.; Kageyama, T.; Watanabe, J.; Yamakawa, J. *Acta Crystallogr.* **1993**, *C49*, 1275−1277.
(136) Moqine, A.; Boukhari, A.; Darriet, J. *J. Solid State Chem.* **1993**, *107*, 362−367.
(137) Abraham, F.; Ketatni, M.; Mairesse, G. *Eur. J. Solid State Inorg. Chem.* **1994**, *31*, 313−323.
(138) Yamashita, A.; Kawahara, A. *Acta Crystallogr.* **1995**, *C51*, 1483−1485.
(139) Fehlmann, M.; Ghose, S.; Finney, J. J. *J. Chem. Phys.* **1964**, *41*, 1910−1916.
(140) (a) $Ca_3Cu_3(PO_4)_2$: Anderson, J. B.; Kostiner, E.; Ruszala, F. A. *J. Solid State Chem.* **1981**, *39*, 29−34. (b) $Ca_3Cu_3(AsO_4)_2$: Osterloh, D.; Müller-Buschbaum, Hk. *J. Alloys Compd.* **1994**, *206*, 155−158.
(141) Brunel-Laügt, M.; Durif, A. *Acta Crystallogr.* **1974**, *B30*, 2118−2121.
(142) Brunel-Laügt, M.; Tordjman, I. *Acta Crystallogr.* **1976**, *B32*, 203−205.
(143) Heide, G. H.; Boll-Dornberger, K. *Acta Crystallogr.* **1955**, *8*, 425−430.
(144) Effenberger, H. *J. Alloys Compd.* **1996**, *233*, 107−111.
(145) (a) Toman, K. *Acta Crystallogr.* **1977**, *B33*, 2628−2631. (b) Toman, K. *Acta Crystallogr.* **1978**, *B34*, 715−721. (c) Burn, P.; Hawthorne, F. C. *Canadian Mineralogist* **1995**, *33*, 885−888.
(146) Poulsen, S. J. Calvo, C. *Canad. J. Chem.* **1968**, *46*, 917−927.
(147) Hawthorne, F. C. *Am. Mineral.* **1986**, *71*, 206−209.
(148) Etheredge, K. M. S., Ph.D. Dissertation, Rice University, 1996.
(149) Wardojo, T. A.; Mackay, R.; Ulutagay, M.; Etheredge, K. M. S.; Hwu, S.-J. *J. Am. Chem. Soc.*, to be submitted 1998.
(150) Wardojo, T. A., M.A Thesis, Rice University, 1996.
(151) Greenwood, N. N.; Earnshaw, A. *Chemistry of the Elements*; Pergamon Press: Oxford, 1984; pp 1366−1368.
(152) Shannon, R. D. *Acta Crystallogr.* **1976**, *A32*, 751−767.
(153) Reim, J.; Griesar, K.; Haase, W.; Krebs, B. *J. Chem. Soc., Dalton Trans.* **1995**, 649−656.
(154) (a) Carlin, R. L. In *Magnetochemistry*; Spring-Verlag: Berlin 1986; p 206. (b) Adams, R. D.; Layland, R.; Datta, T.; Payen, C. *Polyhedron* **1993**, *12*, 2075−2077. (c) Conklin, B. J.; Sellers, S. P.; Fitzgerald, J. P.; Yee, G. T. *Adv. Mater.* **1994**, *6*, 836. (d) Adam, R. D.; Layland, R.; Payen, C. *Inorg. Chem.* **1995**, *34*, 5397−5398.
(155) (a) Etheredge, K. M. S.; Hwu, S.-J. *Inorg. Chem.*, **1995**, 34, 5013−5016. (b) Hase, M.; Etheredge, K. M. S.; Hwu, S.-J.; Shirane, G. *Phys. Rev. B.*, **1997**, *56*, 3231−3238.
(156) Etheredge, K. M. S.; Hwu, S.-J. *Inorg. Chem.* **1996**, *35*, 5278−5282.
(157) For example: Zhang, Y.; Warren, C. J.; Haushalter, R. C.; Clearfield, A.; Seo, D.-K.; Whangbo, M.-H. *Chem. Mater.* **1998**, *10*, 1059−1064.
(158) (a) Goodenough, D. L. *Magnetism and the Chemical Bond*; Interscience: New York, 1963. (b) Hay, P. J.; Thibeault, J. C.; Hoffmann, R. *J. Am. Chem. Soc.* **1975**, *97*, 4884−4899.

CM980232L